Dominik Lechleitner, BSc

Design Method for Optimized Gearboxes in Electric Vehicles

MASTER'S THESIS

to achieve the university degree of

Diplom-Ingenieur

Master's degree programme: Mechanical Engineering

submitted to

Graz University of Technology

Supervisor

Assoc.Prof. Dipl.-Ing. Dr.techn. Mario Hirz

Institute of Automotive Engineering

Second Supervisor

Dipl.-Ing. Martin Hofstetter

Graz, June 2019

Acknowledgement

This thesis would have never come together without the help and guidance of some respected persons, who deserve my deepest gratitude. A few of them I want to address here.

My sincere thanks go to my mentor, Martin Hofstetter, who was a reliable and rich source of wisdom to me during the past two years and never hesitated to provide support when needed. I would also like to thank my supervising professor, Mario Hirz, for his valuable guidance and trust in me.

Special thanks to everybody I had the joy of working with at Magna Powertrain. Their valuable inputs formed the foundation of this thesis and their continuing cooperation and trust in my work were highly encouraging.

I would also like to thank the developer team of FreeCAD – under the guidance of Jürgen Riegel, Werner Mayer and Yorik van Havre – for providing a free and integrable CAD software, which proved to be most valuable for my work. In addition, special thanks to Steven G. Johnson for providing the free nonlinear optimization package NLopt, which I found very useful for my thesis.

Last but not least, I would like to thank my parents, Josef and Karin Lechleitner, for their remarkable support throughout the years of my studies. This journey would have never been possible without their continuing encouragement.

Affidavit

I declare that I have authored this thesis independently, that I have not used other than the declared sources/resources, and that I have explicitly indicated all material which has been quoted either literally or by content from the sources used. The text document uploaded to TUGRAZonline is identical to the present master's thesis.

May 22nd, 2019 

....

Date Signature

Abstract

Driven by the need for clean and sustainable mobility, the demand for alternative drive systems for vehicles is continuously rising. The high degree of innovation of such systems combined with short development cycles confronts automotive manufacturers with a complex problem in the design process. Considering all product requirements, conventional design strategies reach their limits.

In order to overcome these limits, the present thesis introduces a design method in particular for gearboxes in electrified drive systems. The gearbox is the linking element between electric machine and drive shafts of the wheels and thus a vital part in electric powertrains. To reduce the perceived problem complexity, a holistic multi-objective optimization strategy is applied, which supports the product development process in the early phases. The approach on system level "gearbox" considers the interactions between single components like shafts, gear wheels, bearings and housing, which permits to find global design optima. By applying an evolutionary algorithm, the computer-aided synthesis process is able to pursue a variety of even conflicting design goals based on a requirements catalog. Exemplary, mass, costs, efficiency and package integration of the gearbox are optimized. Apart from that, the method is able to apply a common-part strategy, which permits the minimization of production and logistics costs for future gearboxes. The gearbox properties are determined based on current industry standards and guidelines as well as a 3D-CAD software to maximize the accuracy and quality of the result.

The application of the described method is demonstrated based on two case studies. The results are embodied by Pareto fronts of optimal gearbox designs from which decision makers are able to select the most promising solutions. Accordingly, with the presented method a reduction of development time and risk can be expected, which leads to improved quality, efficiency and effectiveness in the early development phases.

Kurzfassung

Getrieben durch die Notwendigkeit sauberer und nachhaltiger Mobilität steigt der Bedarf an alternativen Antriebssystemen im Straßenverkehr stetig an. Der hohe Innovationsgrad solcher Systeme verbunden mit kurzen Entwicklungszeiten stellt Automobilhersteller vor ein äußerst komplexes Problem im Entwicklungsprozess. Unter Einbeziehung aller Produktanforderungen stoßen konventionelle Auslegungsstrategien hierbei an ihre Grenzen.

Um diese Grenzen zu überwinden, beschäftigt sich die vorliegende Masterarbeit mit einer Auslegungsmethode speziell für Getriebe in elektrifizierten Antrieben. Das Getriebe stellt das Verbindungsglied zwischen elektrischer Maschine und Antriebswellen der Räder dar und ist somit ein zentrales Element im Antriebsstrang. Um die Problemkomplexität beherrschbar zu machen, wird eine ganzheitliche, multikriterielle Optimierungsstrategie verfolgt, welche den Produktentstehungsprozess in der frühen Entwicklungsphase unterstützt. Der holistische Ansatz auf Systemebene „Getriebe“ berücksichtigt dabei die Wechselwirkungen einzelner Komponenten, wie Wellen, Zahnräder, Lager und Gehäuse, womit global optimale Getriebedesigns gefunden werden können. Der auf einem evolutionären Algorithmus basierende und computergestützte Syntheseprozess ist dabei in der Lage, ausgehend von einem Anforderungskatalog mehrere auch in Konflikt stehende Auslegungsziele zu verfolgen. So werden beispielsweise Masse, Kosten, Effizienz und Bauraumintegration des Getriebes optimiert. Darüber hinaus ist es möglich, durch Einsatz einer Gleichteilestrategie die Produktions- und Logistikkosten für zukünftige Getriebe zu minimieren. Zur Bestimmung der Getriebeeigenschaften wird auf anerkannte Normen und Richtlinien sowie eine 3D-CAD-Software zurückgegriffen, um die Genauigkeit und Qualität des Ergebnisses zu maximieren.

Die Anwendung der beschriebenen Methode wird anhand zweier Fallstudien demonstriert. Als Resultat werden Pareto-Fronten von Getriebevarianten generiert, aus welchen Entscheidungsträger die vielversprechendsten Lösungen auswählen können. Somit ist zu erwarten, dass sich durch Einsatz der vorgestellten Methode sowohl Entwicklungszeit als auch -risiko verringern lassen, was zu deutlich gesteigerter Qualität, Effizienz und Effektivität in der frühen Entwicklungsphase führt.

Contents

Abbreviations

BEV	Battery electric vehicle
CAD	Computer-aided design
CRB	Cylindrical roller bearing
DIN	Deutsches Institut für Normung
EV	Electric vehicle
FCEV	Fuel cell electric vehicle
GBB	Grooved ball bearing
HEV	Hybrid electric vehicle
ICE	Internal combustion engine
ISO	International Organization for Standardization
MBSE	Model-based systems engineering
NVH	Noise, vibration, harshness
OEM	Original equipment manufacturer
PHEV	Plug-in hybrid electric vehicle
RFLP	Requirements, Functional, Logical, Physical
TRB	Tapered roller bearing
VG	Viscosity grade
WLTC	Worldwide Harmonized Light Vehicles Test Cycle
WLTP	Worldwide Harmonized Light Vehicles Test Procedure
e-drive	Electric drive unit
rpm	Revolutions per minute

Symbols

Latin, uppercase

C	Costs
C_0	Reference costs
$C_{0\mathrm{r}}$	Static load rating of a radial bearing
C_r	Dynamic load rating of a radial bearing
F	Force
F_{Br}	Radial bearing reaction force
F_{Bx}	x-component of bearing reaction force
F_{By}	y-component of bearing reaction force
F_{ByTot}	Sum of all F_{By} for a shaft support
F_{Bz}	z-component of bearing reaction force
F_t	Tangential force at the reference diameter of a gear wheel
F_u	Unit force
F_{Wa}	Axial force at the pitch point of a gear wheel
F_{Wr}	Radial force at the pitch point of a gear wheel
F_{Wt}	Tangential force at the pitch point of a gear wheel
F_{Wx}	x-component of a gear force at the pitch point
F_{Wz}	z-component of a gear force at the pitch point
H_V	Gear power loss factor
K_A	Application factor
$K_{\mathrm{F}\alpha}$	Transverse load factor for tooth root stress
$K_{\mathrm{F}\beta}$	Face load factor for tooth root stress
$K_{\mathrm{H}\alpha}$	Transverse load factor for contact stress
$K_{\mathrm{H}\beta}$	Face load factor for contact stress
K_V	Dynamic factor
L_B	Fatigue lifetime of a bearing
L_ref	Reference load
$P_{0\mathrm{r}}$	Combined static radial bearing load
P_l	Determining bearing load for the power loss calculation
P_in	Gearbox input power
P_l	Gearbox power loss
$P_{\mathrm{GP\,in}}$	Input power of a gear pair
$P_{\mathrm{l\,B}}$	Total Power loss of a bearing
$P_{\mathrm{l\,B\,L}}$	Load-dependent power loss of a bearing
$P_{\mathrm{l\,B\,V}}$	Velocity-dependent power loss of a bearing

$P_{\mathrm{l\,GP}}$	Total power loss of a gear pair
$P_{\mathrm{l\,GP\,L}}$	Load-dependent power loss of a gear pair
$P_{\mathrm{l\,GP\,V}}$	Velocity-dependent power loss of a gear pair
$P_{\mathrm{l\,RSS}}$	Total power loss of a radial shaft seal
P_{r}	Combined dynamic radial bearing load
$P_{\mathrm{r\,eq}}$	Equivalent combined dynamic radial bearing load
Q_{D}	Diameter ratio
S_0	Safety factor for the static load capacity of a bearing
S_{F}	Safety factor for root bending strength of a gear wheel
S_{H}	Safety factor for flank surface durability of a gear wheel
T	Torque
T_{GP}	Torque acting on wheel 1 of a gear pair
T_{in}	Gearbox input torque
T_{nom}	Nominal torque transmitted by a shaft
T_{shaft}	Sum of all action torques on a shaft
T_{u}	Unit torque
U	Damage sum according to Palmgren-Miner
V_{approx}	Approximated volume of a shaft component
V_{iAvail}	Protruding powertrain volume with respect to the available installation space
V_{iForb}	Intersecting powertrain volume with the forbidden installation space
W_{in}	Gearbox input work in a driving cycle
W_{l}	Gearbox energy loss in a driving cycle
X	Calculation factor for P_{r}, radial
X_0	Calculation factor for $P_{0\mathrm{r}}$, radial
X_1	Calculation factor for P_1, radial
Y	Calculation factor for P_{r}, axial
Y_0	Calculation factor for $P_{0\mathrm{r}}$, axial
X_1	Calculation factor for P_1, axial
Y_{B}	Rim thickness factor
Y_{DT}	Deep tooth factor
Y_β	Helix angle factor for tooth root stress
Y_{F}	Form factor
Y_{S}	Stress correction factor
Z_β	Helix angle factor for contact stress
Z_{E}	Elasticity factor
Z_ε	Contact ratio factor
Z_{H}	Zone factor

Latin, lowercase

a_1	Failure probability factor
a_{ISO}	Stress-lifetime modification factor

a_{tot}	Total center distance of the gearbox
b	Face width of a gear wheel
b_{h}	Width of a gear wheel at the hub
b_{s}	Web thickness of a gear wheel
c	Mass-specific cost factor
c_{Avail}	Minimum clearance of the powertrain to the installation space surface
c_{B1G1}	Axial distance between bearing 1 and gear wheel 1
c_{G2G3}	Axial distance between gear wheels 2 and 3
d	Reference diameter of a gear wheel
d_{a}	Tip diameter of a gear wheel
d_{f}	Root diameter of a gear wheel
d_{i}	Inner diameter of a gear wheel
d_{inner}	Inner shaft diameter
d_{M}	Mean bearing diameter
d_{outer}	Outer shaft diameter
d_{RSS}	Diameter of a radial shaft seal at the sealing point
d_{W}	Pitch diameter of a gear wheel
f	Objective function
f_0	Velocity-dependent friction coefficient of a bearing
f_1	Load-dependent friction coefficient of a bearing
g	Inequality constraint
h	Equality constraint
i_{GP}	Transmission ratio of a gear pair
i_{tot}	Total transmission ratio of the gearbox
m	Mass
m_{n}	Normal module of a gear wheel
n	Rotational velocity
n_{B}	Rotational velocity of a bearing
n_{eq}	Equivalent rotational velocity
n_{F}	Number of action forces acting on a shaft assembly
n_{GP}	Number of gear pairs
n_{LB}	Number of bins in a load spectrum
n_{LC}	Number of load cycles for a bin in the load spectrum
$n_{\mathrm{LC\,lim}}$	Maximum number of load cycles before failure occurs
n_{P}	Quantity of a purchased or produced product
n_{P0}	Reference quantity of a purchased or produced product
p	Slope of the stress-cycle curve
p_{B12S}	Selection parameter for bearings 1 and 2
p_{B2T}	Type parameter for bearing 2
p_{B34S}	Selection parameter for bearings 3 and 4
p_{B34T}	Type parameter for bearings 3 and 4
p_{B56S}	Selection parameter for bearings 5 and 6

p_{B56T}	Type parameter for bearings 5 and 6
p_{Forb}	Penalty factor for intersections with the forbidden installation space
q	Time slice ratio
q_{PM}	Package metric
$q_{\mathrm{PM\,min}}$	Minimum package metric for a certain powertrain configuration
r^*	Coordinate direction in the unwound radial projection
s_{h}	Hub thickness of a gear wheel
s_{r}	Rim thickness of a gear wheel
t_{PE}	Tangential offset of the power electronics
u	Tooth ratio
x	Optimization parameters, profile shift coefficient, coordinate direction
x_{IS0}	x-direction of the installation space system
x_{L}	x-coordinate of an action force application point
x_{PT0}	x-direction of the powertrain system
x_{W}	x-coordinate of the pitch point of a gear wheel
y	Coordinate direction
y_{BL}	y-coordinate of a bearing force application point
y_{IS0}	y-direction of the installation space system
y_{L}	y-coordinate of an action force application point
y_{PE}	Axial offset of the power electronics to the front face of the electric machine
y_{PT}	Axial offset of the powertrain
y_{PT0}	y-direction of the powertrain system
y_{wo}	Axial web-offset of a gear wheel
z	Number of teeth of a gear wheel, coordinate direction
z_{IS0}	z-direction of the installation space system
z_{L}	z-coordinate of an action force application point
z_{PT0}	z-direction of the powertrain system
z_{W}	z-coordinate of the pitch point of a gear wheel

Greek, uppercase

Θ_{ISdir}	Alignment direction of the intermediate shaft
Θ_{PE}	Arrangement angle of the power electronics
Θ_{PT}	Tilt angle of the powertrain
Θ_{SA}	Arrangement angle between shaft assemblies
Ψ_{D}	Face width to diameter ratio of a gear wheel

Greek, lowercase

α_{Wt}	Operating pressure angle in transverse plane
β	Helix angle at the reference diameter
β_{1dir}	Helix angle direction of gear wheel 1
β_{b}	Helix angle at the base diameter
β_{W}	Helix angle at the pitch diameter
ε_1	Contact ratio tooth tip
ε_2	Contact ratio tooth root
ε_α	Transverse contact ratio
ε_β	Overlap ratio
η	Degree of gearbox efficiency
ϑ_{oil}	Oil temperature
λ	Degree of gearbox losses
μ_{mZ}	Mean gear friction coefficient
ν	Kinematic oil viscosity
ν_{40}	Nominal kinematic oil viscosity at 40 °C
ρ	Density
σ_{H}	Contact stress at the tooth flank
σ_{F}	Tensile stress at the tooth root
τ_{p}	Permissible nominal torsional stress of a shaft

1 Introduction

Around the globe continuing efforts are made to reduce the environmental impact of road traffic. Measured only by the carbon dioxide emissions, road vehicles account for 17.5 % of the total global emissions, which is seven times higher than for sea and air traffic [1]. Efforts exemplary include tightening the fuel economy and emission standards, China's "New Energy Vehicle" quota, purchase incentives for electric vehicles (EVs) and local bans for fossil fuel cars [4].

In order to adapt to the resulting market changes, automotive original equipment manufacturers (OEMs) follow plans towards a large-scale powertrain electrification of their product lines - thus employing an alternative drive system that can purly rely on renewable and sustainable energy. That way, current predictions indicate a global share of 55 % of all new car sales and a share of 33 % of the global car fleet for EVs by 2040 (Figure 1.1) [4].

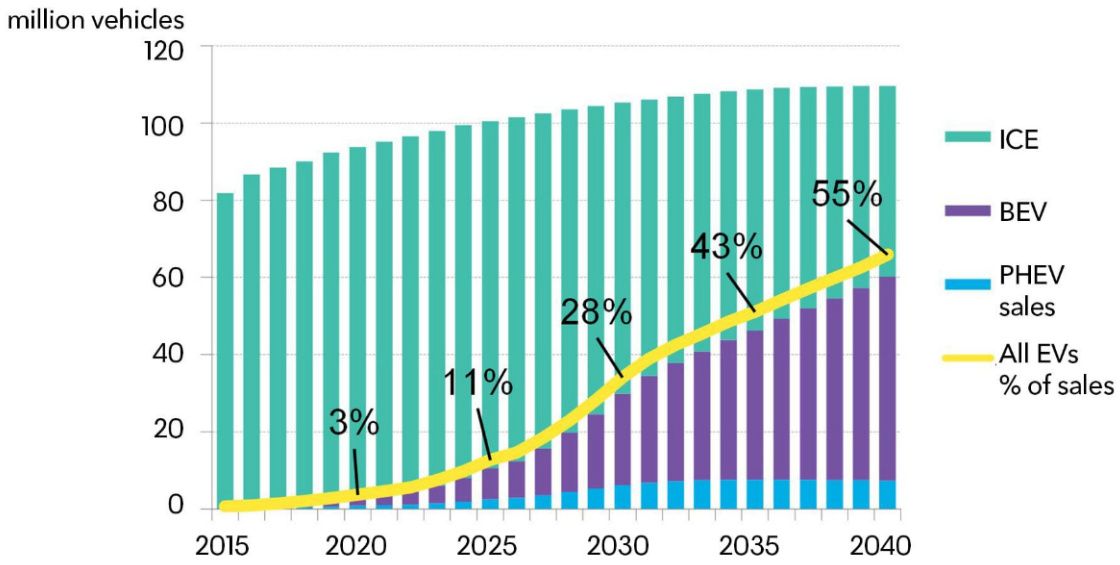

Figure 1.1: Predicted annual global light duty vehicle sales, [4]

The radical change from combustion-based propulsions to electrified powertrains induces a high degree of innovation in the development of such systems. Combined with the short development cycles required by the market, engineers are facing a complex problem in

the design process of EVs. This leads to situations where conventional design methods reach their limits.

The purpose of this thesis is to develop a design method that is capable of handling this complexity and find global optimal design solutions for gearboxes in electrified vehicles. To achieve this, a design process based on a holistic multi-objective optimization strategy is presented.

For that purpose, section 2 gives an overview of electrified powertrains and gearboxes in such systems. Furthermore, design strategies and the application of optimization algorithms to perform design tasks are discussed. Section 3 explains the chosen approach including the used analysis models and optimization strategy. Finally, section 4 demonstrates the application of the presented method based on two case studies. The results are discussed and compared to fully engineered reference designs.

Previous findings originating from work on this thesis have already been published in [16]. However, especially the required analysis models (gearbox calculation schemes and package rating) have been refined since.

2 Theory & Literature Discussion

The following section is intended to give an overview of electrified powertrains and especially the system "gearbox". Furthermore, strategies for designing such a system are outlined and the application of optimization algorithms to perform the corresponding design task is discussed.

2.1 Gearboxes in Electrified Vehicles

An electrified powertrain uses an electric traction motor and possibly other machines, like internal combustion engines, to drive a vehicle. When braking, the electric motor can be used as generator for recuperating energy. Thus, the traction motor/generator is further generically referred to as "electric machine".

Manifold electrified powertrain solutions are thinkable and in fact also exist. The most common topologies employ an internal combustion engine (ICE) combined with one or more electric machines or purely rely on one or more electric machines. The former topologies are used in hybrid electric vehicles (HEV), the latter ones in battery electric vehicles (BEV) and fuel cell electric vehicles (FCEV), where these two types only differ concerning their energy storage system.

Hybrid electric vehicles mainly profit from lower fuel consumptions and/or lower exhaust emissions compared to vehicles only driven by internal combustion engines. This is achieved by shifting the load from the ICE to the electric machine and vice versa, which allows the ICE to run at a more favorable operating point. Besides the already mentioned increased efficiency and lower emissions, they combine the advantages of high range and fast refueling of ICE-based propulsions with the torque characteristics and regenerative-braking-ability of electric machines. However, hybrid vehicles are more expensive than classical ICE-based ones and, when using fossil fuel, show limited suitability for clean and sustainable road traffic. [34, 38]

Concerning HEVs, the design method presented in this thesis is directly applicable for axle-split hybrids. They use separate propulsion systems for each axle of the vehicle. Typically, the ICE and possibly an electric machine is driving the front axle and a pure electric drive unit the rear axle without any mechanical connecting elements (see Figure 2.1). Topologies only using electric machines on one axle are referred to as "P4" [34]. Among other aspects, such designs are of strategical interest for OEMs as existing car designs employing an internal combustion engine at the driving axle can be

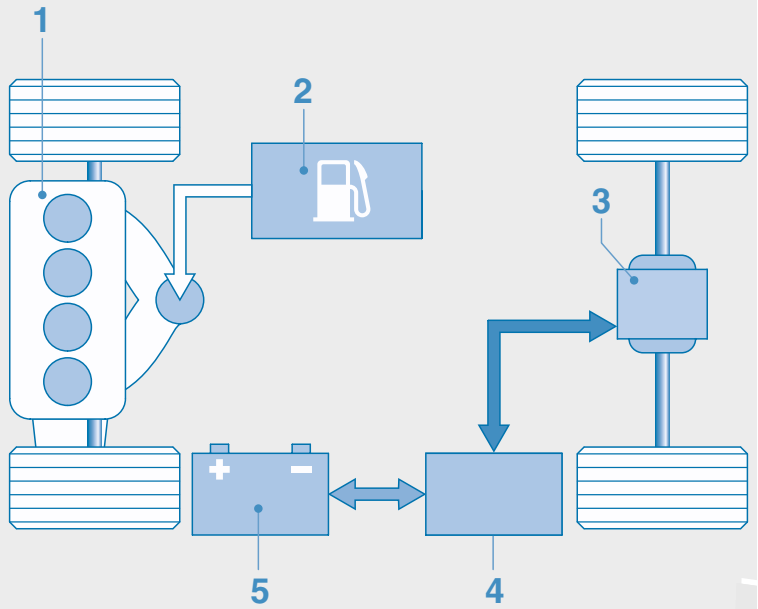

Figure 2.1: Schematic of a P4 hybrid powertrain, [33, page 19];
1) internal combustion engine, 2) fuel tank, 3) electric machine and gearbox, 4) power electronics unit, 5) battery

refitted with an electric drive system at the other axle and thus easily transformed into a hybrid electric vehicle. Except for the advantage of an all-wheel-drive configuration, technologically speaking this topology is mostly suboptimal compared to other hybrid powertrains. Exemplary, the electric machine cannot function as generator when the vehicle is standing still and the power from the ICE to the electric machine is transmitted by the wheels (e.g. unfavorable regarding tire wear, efficiency and vehicle dynamics) [33]. To overcome the disadvantages, the ICE-driven axle of a P4-hybrid can also be equipped with an electric machine, resulting in a combined hybrid electric powertrain [34].

Battery and *fuel cell electric vehicles* purely rely on one or more electric machines to drive the vehicle. One or both axles of the vehicle are equipped with an electric drive unit (analogous to the electric axle of a P4-hybrid). Such propulsion systems are locally emission-free and the energy required can be sustainably produced from renewable resources. The presented design method is applicable for both types of vehicle concepts.

Although it would be interesting to discuss strength and weaknesses of single concepts, well-to-wheel considerations and other system aspects at this point, this goes beyond the scope of the present thesis. The interested reader is referred to the literature, e.g. [33, 34, 38].

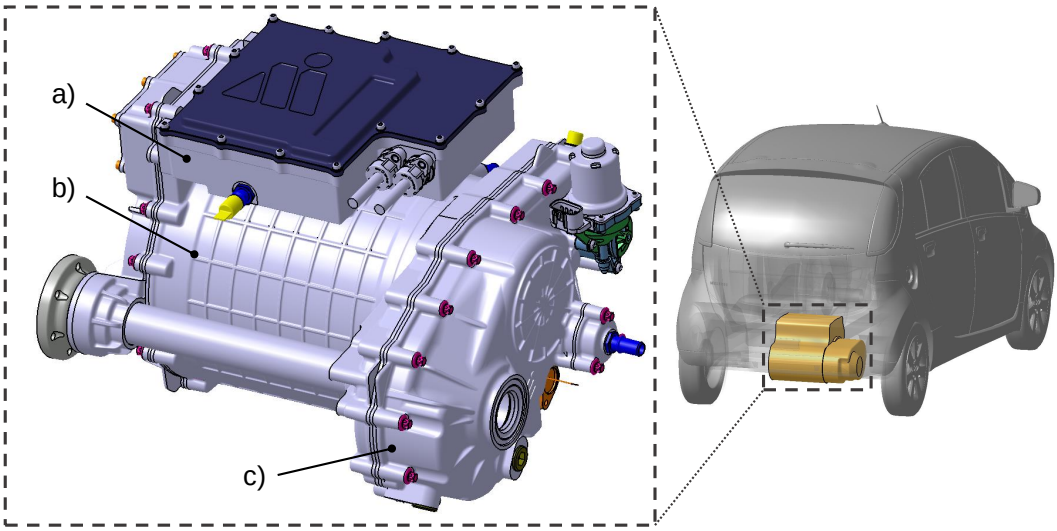

Figure 2.2: CAD-visualization of an e-drive; a) power electronics unit, b) electric machine, c) gearbox

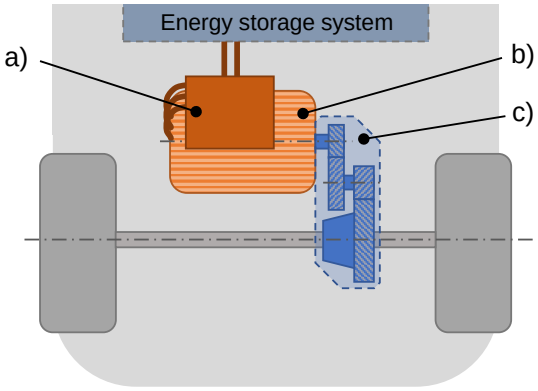

Figure 2.3: Schematic illustration of the main e-drive components; a) power electronics unit, b) electric machine, c) gearbox

System Architecture of E-Drives

An electric drive unit, also referred to as an e-drive, consists of three main components, illustrated in Figure 2.2 and 2.3:

a) Power electronics unit,

b) electric machine and

c) gearbox.

The *power electronics unit*, sometimes not very accurately referred to as ”inverter”, serves

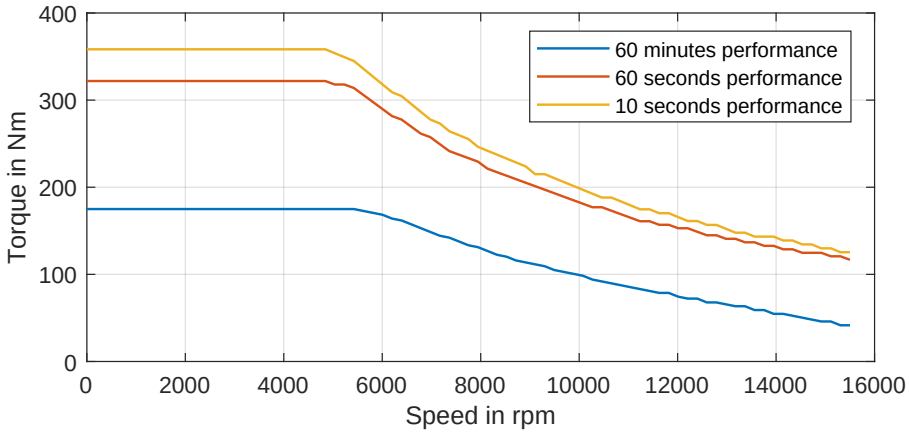

Figure 2.4: Torque-speed characteristic of the electric machine used in case study A (section 4.1)

as interface to the energy storage system. In battery electric vehicles this is a battery providing a direct current. The task of the power electronics unit is to provide an alternating current with proper amplitude, phase and frequency for the electric machine depending on the driving situation (torque and velocity). During regenerative braking, the energy flow direction is reversed. In that case the unit has to convert the alternating current to a direct one suitable to charge the battery.

The *electric machine* is typically a synchronous or asynchronous machine both serving as motor and generator [38]. It has the task to convert the electrical energy provided by the energy storage system and power electronics unit to mechanical energy driving the vehicle – and vice versa during regenerative braking. Due to considerations regarding package, moment of inertia and costs, high-speed machines are favored in e-drives [11]. They are characterized by small diameters and low torque outputs. In order to provide sufficient power to drive the vehicle, such machines thus need to rotate at a high speed. An exemplary torque-speed characteristic of such an electric machine is shown in Figure 2.4. Depending on the time range, the machine is able to output different maximum torques due to thermal limitations. Currently, peak rotational speeds are around 15 000 rpm for high-voltage applications [31].

Driving the wheels at this high velocity is unsuitable since their rotational speed at maximum vehicle velocity typically is below 2 000 rpm. Thus, a *gearbox* is required that reduces the velocity and at the same time increases the torque. The transmission ratios used in the two case studies presented in section 4 are around nine and eleven. As a rule of thumb, the transmission ratio of a single gear stage should be chosen to be equal to or smaller than eight [24], implying that for these transmission ratios a gearbox with at least two stages is required. Electric machines in general show a much wider speed range than internal combustion engines, meaning shiftable multi-speed transmissions are not necessarily required in e-drives. However, two-speed gearboxes may be of interest

e.g. when high maximum vehicle speeds or high torques at low velocities are required (commercial vehicles, off-road vehicles, short 0 - 100 km/h time et cetera). Additionally, with multi-speed transmissions the operating point of the electric machine can be shifted to the most favorable region regarding efficiency depending on the driving situation. This results in a higher total degree of efficiency of the e-drive than for single-speed transmissions [11].

A Closer Look on EV-Gearboxes

Analyzing the interfaces of the gearbox system to the interfering elements, i.e. the electric machine, the drive shafts of the wheels and the vehicle itself, reveals that the main interactions can be described by certain torques, speeds, diameters and the provided as well as required installation space (see Figure 2.5). The electric machine imposes a torque and rotational speed on the gearbox, which are then transformed and transmitted to the drive shafts. Furthermore, the shaft of the electric machine and the drive shafts of the wheels require a certain diameter at the interface to the gearbox system, meaning geometric compatibility needs to be ensured by the gearbox (e.g. see Figure 2.9 for a schematic illustration of possible design variants of the gearbox input shaft). Additionally, the outer diameter of the electric machine (assuming its shape is a right circular cylinder) may impose limitations on possible shapes of the gearbox and its total center distance. Exemplary, for a gearbox with an offset output shaft, the differential might clash with the electric machine depending on its arrangement (see Figure 2.10) or the electric machine might intersect the drive shafts if the total center distance is too small. Lastly, a certain installation space for the gearbox is provided by the vehicle that the gearbox system can utilize. Other, less trivial interactions include thermal aspects (e.g. heat exchange between electric machine and gearbox) and the vibration behavior of the e-drive system including its suspension – especially regarding noise, vibration, harshness (NVH).

Even for single-speed gearboxes, a multitude of gearbox concepts can be applied. Figure 2.6 shows a schematic illustration of some examples including

a) a helical gearbox with an offset output shaft,

b) a helical gearbox in coaxial arrangement,

c) a planetary gear and

d) a combination of a helical and planetary gear stage.

Concerning the latter, a two-stage gearbox design employing a planetary gear for the first and a helical gear pair for the second stage is presented in [31]. As for ICE-based propulsion systems, all listed concepts require a differential, which allows the drive shafts to rotate at different speeds (e.g. when cornering). However, in case the traction on one wheel is low (e.g. one wheel on slippery road surface), the differential limits the utilizable power of the electric machine, which can be avoided by application of a locking

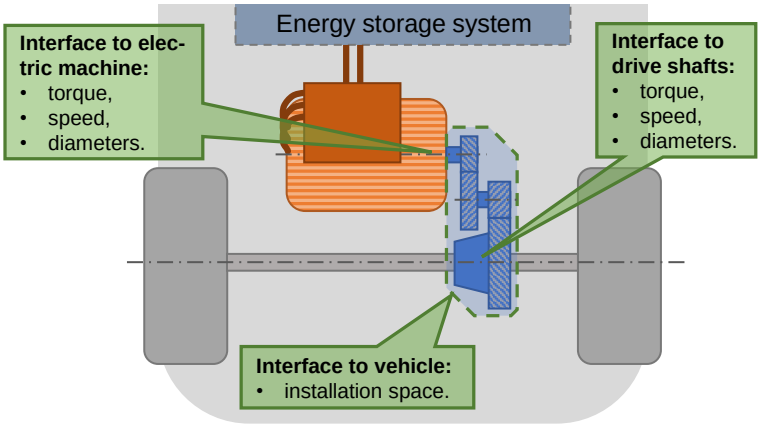

Figure 2.5: Main aspects of the interfaces between gearbox and electric machine, gearbox and drive shafts as well as gearbox and vehicle

differential [13]. The main differences between gearboxes based on helical and planetary gears are their costs and installation space demand. Planetary gears in general are more expensive than helical ones but they also show a more compact shape [13]. However, restrictions concerning their axial length can be more critical [14]. The difference between offset and coaxial designs primarily affects the arrangement of the electric machine and thus packaging aspects – for the former the electric machine is always off-center with respect to the drive shafts, for the latter it is always coaxial.

Apart from e-drives using only one electric machine, special gearbox concepts can be applied for designs with two electric machines (also referred to as "twin" arrangement [31]). For such designs both wheels of the axle are driven independently, allowing for purely electric torque vectoring [13] and eliminating the necessity of a differential. Analogous to concepts with a single electric machine and a non-locking differential, a low traction on one wheel limits the utilizable driving power of the corresponding electric machine. To overcome this, the e-drive can be equipped with a locking clutch, which mechanically connects both shafts in a controlled manner and the axle functions like one with a locking differential. Two examples are shown in Figure 2.7. The first one uses helical gearboxes with offset output shaft for both electric machines, the second one shows a design with planetary gears. Their main differences are analogous to the ones for e-drive designs with a single electric machine.

Although even more concepts than shown in Figures 2.6 and 2.7 are thinkable (especially concerning multi-speed transmissions), the variety of the most commonly used gearbox concepts is limited. Listed in Table 2.1 are the top five EVs (including BEVs, FCEVs and HEVs) sold in the European market in 2017. All of these models make use of a single-speed, two-stage, helical gearbox with offset output shaft and integrated differential, which corresponds to variant a) in Figure 2.6. Thus, this design represents a very common topology for e-drives and is further discussed in greater detail. The interior of

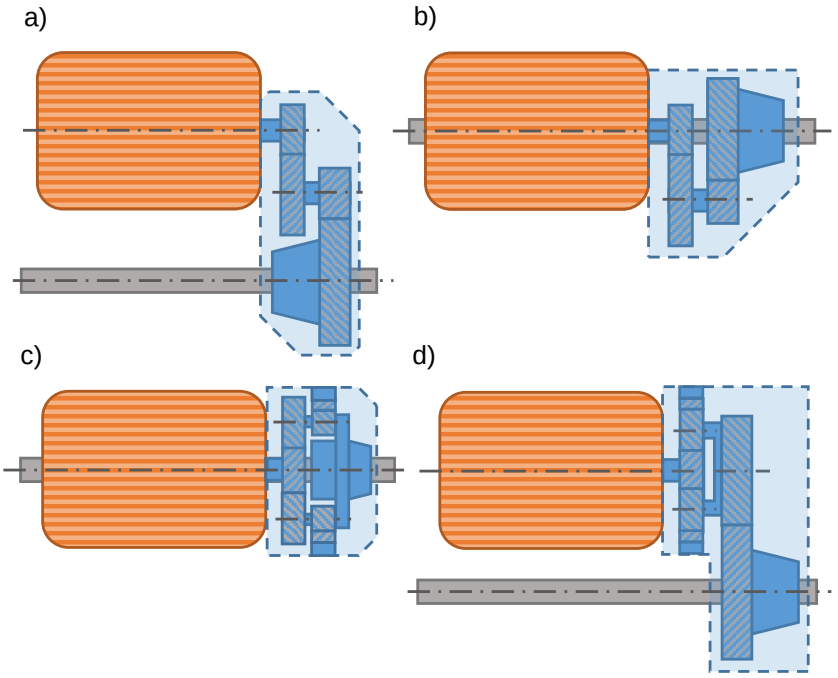

Figure 2.6: Exemplary gearbox concepts for e-drives with a single electric machine; a) offset helical gearbox; b) coaxial helical gearbox; c) planetary gears; d) combination of helical and planetary gear stages [31]

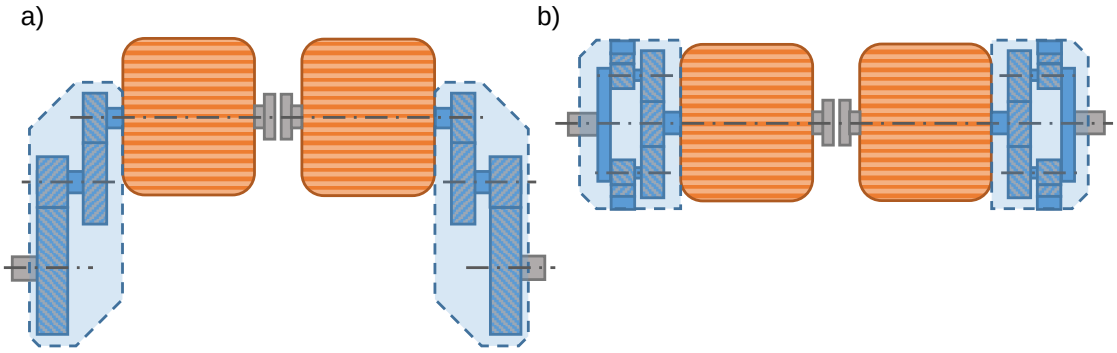

Figure 2.7: Exemplary gearbox concepts for e-drives with two electric machines; a) offset helical gearboxes; b) planetary gears

Table 2.1: Top five EVs sold in Europe in 2017, [2]

Model name	Type	Sales
Renault Zoe	BEV	31 410
BMW i3	BEV	20 855
Mitsubishi Outlander	axle-split HEV	19 189
Nissan Leaf	BEV	17 454
Tesla Model S	BEV	15 553

such a topology is shown in Figure 2.8.

The main components are

a) gear wheels,

b) rolling bearings,

c) shafts,

d) shaft seals and

e) a housing supporting the interior.

Apart from that, additional components and subsystems like lubrication and cooling systems, park locks, sensors and more can be found. Concerning the interface of the gearbox input shaft to the electric machine, an integral or modular design can be chosen as exemplary illustrated in Figure 2.9. An integral design uses a common shaft for the electric machine and the gearbox input shaft, meaning both electric machine and gearbox are not functional as separated systems. This is different for a modular design where both shafts are connected by e.g. a coupling. Such a layout might be of interest for modular design kits for e-drives.

Furthermore, for a single-speed, two-stage, helical gearbox, various arrangement options for the shafts and the differential arise. In total four different arrangements are eligible, schematically illustrated in Figure 2.10. Depending on the arrangement variant, the gearbox-internal load situation (e.g. bearing reaction forces) and especially the installation space demand changes.

2.2 Design Synthesis Strategies

When approaching the task of designing a specific system, a specialized method being able to perform the corresponding design task is needed. The automotive development process on a macroscopic scale often implements the so-called V-model [43]. Originating from software development, it describes major steps that can be taken to obtain a verified product design from a product requirements catalog. A schematic illustration of the V-model is shown in Figure 2.11. A key feature is the system-based approach to the design

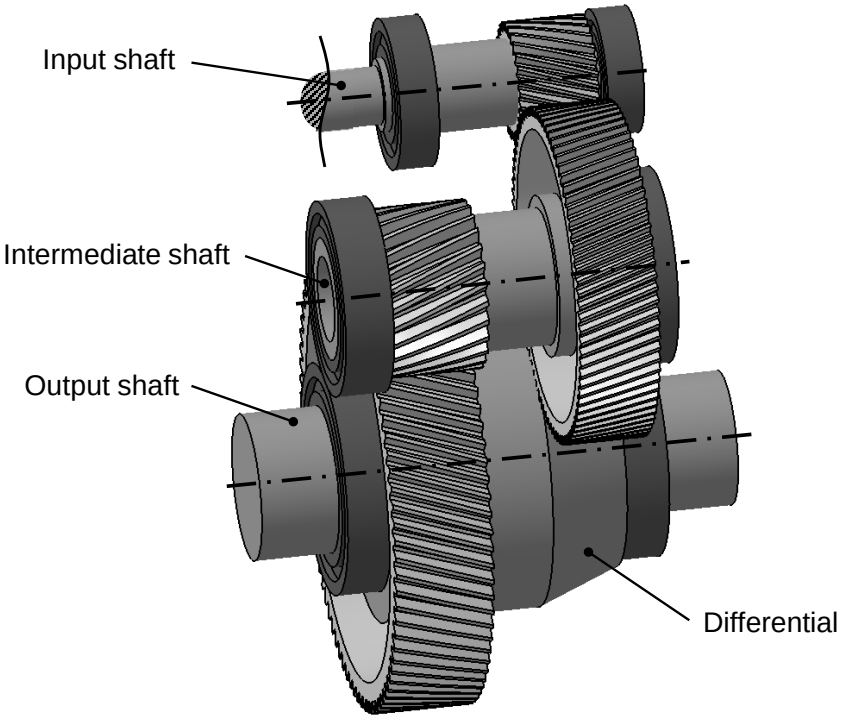

Figure 2.8: CAD-visualization of the interior of an exemplary single-speed, two-stage, helical offset gearbox with integrated differential

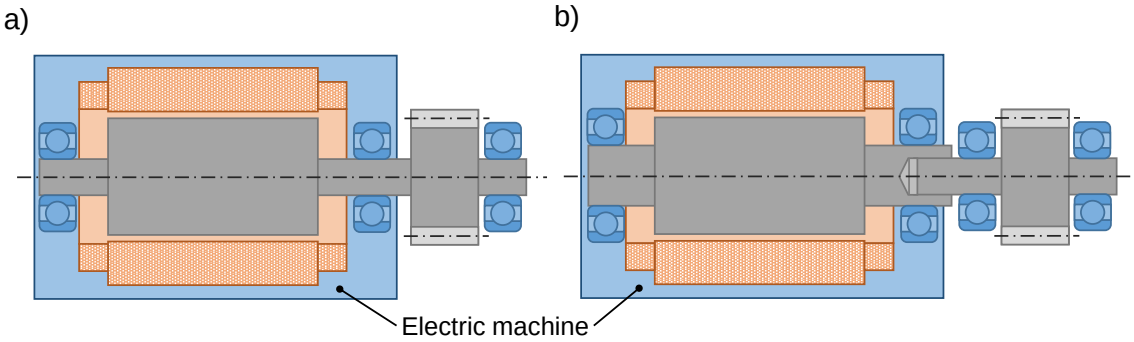

Figure 2.9: Schematic example designs of the gearbox input shaft; a) integral design, b) modular design

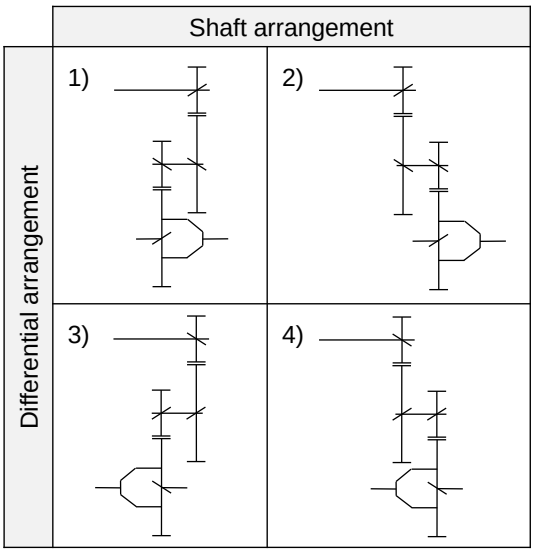

Figure 2.10: Schematic illustration of possible shaft and differential arrangements for a single-speed, two-stage, helical gearbox

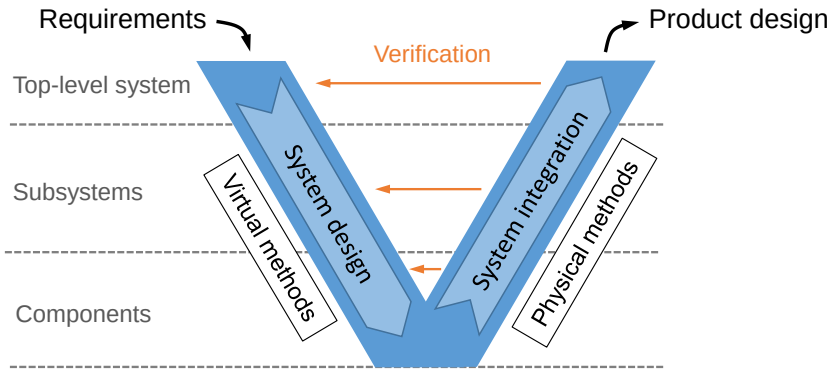

Figure 2.11: Illustration of the V-model

task. Starting from the requirements set on the top-level system – the product itself – necessary subsystems and corresponding requirements are identified. This logic continues down to the component level (e.g. a gear wheel), where basic design decisions are made (e.g. module of a gear wheel). The descending branch of the V-model makes use of virtual methods to design the product, the ascending branch uses physical methods to manufacture and assemble a prototype and to perform experimental testing. The results of these tests – ultimately performed at the top-level system – give reliable indications if the product requirements are fulfilled or not. [27, 43]

However, prototype-based tests are expensive. If the outcome of such a test is unsatisfactory, the design has to be adapted and the V-model, at least partially, run through

again – which again causes costs and is time consuming. This is why continuing efforts are made to replace these physical tests by virtual ones as early as possible in the development process. Shifting development efforts from the ascending to the descending branch of the V-model is called "frontloading" [43]. Emphasizing on virtual product development requires sophisticated models of the product to be designed. Such models are an abstraction and thus a virtual representation of the real product described by scientific laws. Especially in the context of complex systems, the discipline of model-based systems engineering (MBSE) arises [17]. The design method described in this thesis also uses a MBSE-based approach to support the virtual product development in the early stages of the product development process.

From Requirements to Product Design

Various microscopic methods are applied throughout the V-model to perform the design tasks, which is solving the actual design problems. In the context of the present thesis, a design problem consists of requirements (e.g. minimum mass) and design parameters (e.g. number of teeth of a gear wheel) which fully describe the product configuration. The design task is to find design parameters so that the resulting product design fulfills the given requirements best.

The corresponding design methods and the underlying design processes can be distinguished according to the used strategy into implicit and explicit methods [30]. The latter are able to explicitly transform given requirements into required design parameters without the need to iteratively search for a solution. Such methods are fast and mathematically exact. However, for complex design tasks, finding an explicit method comes with huge effort and may be infeasible. Implicit design methods iteratively search for the needed design parameters and thus hardly have any limitations concerning complexity. This is mostly done by implementing a trial and error scheme with the two processes (see Figure 2.12)

a) system analysis and

b) design synthesis [30].

The system analysis process evaluates the system properties (e.g. the mass of the system) based on the chosen design parameters. The design synthesis then uses the result of the system analysis to make design decisions (e.g. increase/decrease number of teeth of a gear wheel) with the aim of finding a design that fulfills the given requirements better than the previously tested one.

The conventional approach to synthesize a design is to rely on one or more skillful engineers, who manually perform and assess the results of the system analysis and make appropriate adaptions to improve the design. This is usually done at the component level by applying heuristic synthesizing strategies. Machine elements commonly found in gearboxes are well examined as isolated components. Highly acknowledged reference

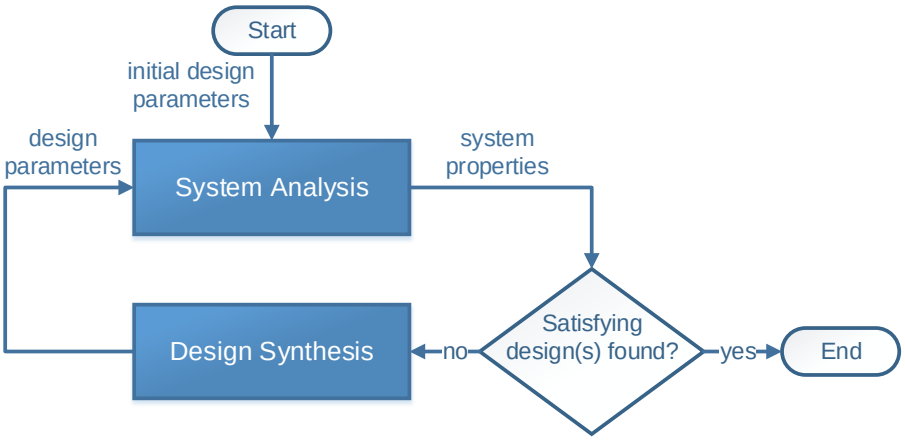

Figure 2.12: Implicit design strategy by iterating analysis and synthesis [30]

works such as [26] give detailed design recommendations on how to select the design parameters of a single component in order to achieve a certain design goal. However, many components coexist in the respective supersystem and their interactions also dictate the system properties. The synthesizing process therefore has to not only consider isolated components but also their interactions in the system context. An illustrative example includes the efficiency optimization of a gearbox. According to [26] an efficient gear design will generally favor high helix angles. Such a design will as a consequence induce high bearing loads, which in turn lead to high frictional losses at the bearings. This exemplary conflict outlines the importance of well-considered synthesizing strategies at component level.

A Holistic Approach to the Design Task

In order to eliminate the necessity of explicitly considering interactions, a holistic approach to the design task is required. This means the system to be designed is described by analysis models implementing all design parameters and exposing all system properties of interest. The interactions of further subsystems and components are thus implicitly described by the analysis models – a change of one or more design parameters directly yields the new system properties. All design decisions are now made at the top-level system, eliminating the need for component design heuristics. On the downside, a synthesizing strategy is now required, which is capable of performing the design task at system level.

However, a design problem can be formulated as an optimization problem, where the design parameters are treated as optimization parameters, the design goals (e.g. minimum costs) as optimization objectives and further requirements as constraints for the optimization. Depending on the design task at hand, a more or less complex optimization problem results, which in general requires sophisticated optimization algorithms

and computers for solving.

2.3 Introduction to Optimization Problems

Mathematically speaking, an optimization problem consists of optimization parameters x, constraints and objective functions f. The optimization parameters form the so-called search space. Constraints in general depend on x, restrict the search space and can be expressed as equalities (2.1) and/or inequalities (2.2). Objective functions (2.3) define the objective space and need to be optimized (either maximized or minimized), which is the actual task of the optimization process. Each maximization problem can be rewritten into a minimization problem by simply changing the sign of the respective objective function and vice versa. The full optimization problem can thus be generically described by the constraints

$$h_j = 0 \quad \text{for } j \in [1, 2, \ldots, J]\,, \tag{2.1}$$

$$g_k \leq 0 \quad \text{for } k \in [1, 2, \ldots, K] \tag{2.2}$$

and the objective function optimization

$$\text{minimize}\,(f_i) \quad \text{for } i \in [1, 2, \ldots, M]\,, \tag{2.3}$$

where J is the number of equality constraints, K is the number of inequality constraints and M is the number of objective functions. The number of independent constraints must be less than or equal to the number of optimization parameters. Otherwise the problem is over-determined and no solution might exist. [6, 25]

For solving an optimization problem, a multitude of algorithms exists and can be distinguished in various ways. In fact, algorithms for optimization are more diverse than the types of optimization problems. However, no single algorithm is well-suited for all problems, as dictated by the No Free Lunch Theorems. [25]

A Glance at Numerical Optimization Algorithms

A first distinction can be made between *derivative-based* and *derivative-free* algorithms. Derivative-based methods are mathematically inspired, as they use the slope information of the objective function to find the minima. Some examples are the classic method of steepest descent and Gauss-Newton. Derivative-free methods do not require the gradient of the objective function and are thus also applicable for problems for which the gradient is unknown or has singularities within the search space. One example of such an algorithm is the popular Nelder-Mead (also referred to as downhill-simplex) method. [25]

Algorithms can further be classified as *trajectory-based* and *population-based*. Trajectory-based methods use a single agent for the optimization, meaning the objective function is evaluated at a single point and the next evaluation point depends on the result of the previous evaluation. That way, starting from an initial point, trajectory-based algorithms trace out a path towards the minima as the optimization process continues. Exemplary, the method "hill-climbing" is trajectory-based, and it links the starting point with the final point via a piecewise zigzag path. Population-based algorithms use multiple agents or individuals – in sum representing the population – for the optimization. The objective function is independently evaluated at multiple points. The result of all evaluations is then used to decide about the next evaluation points. From a computational point of view, good parallelization abilities of population-based algorithms arise. Examples of population-based methods can be found in the vast family of evolutionary algorithms. [25]

Another distinction can be made between *deterministic* and *stochastic* algorithms. The former use a logic without any random nature, meaning that they will always lead to the same result when the same starting points are chosen. The latter incorporate a random behavior with a varying degree – from simply using a random starting point and otherwise deterministic optimization to the also random optimization process of metaheuristics (e.g. evolutionary algorithms). Deterministic algorithms many times do not require a lot of objective function evaluations. This is different for stochastic algorithms, which in general do require many evaluations simply due to probability considerations. From a computational point of view, this is relevant for problems for which the evaluation of the objective function comes with huge computational effort (e.g. expensive simulations). In practice, solving such a problem simply by means of a stochastic algorithm might be too time-consuming. [25]

Furthermore, depending on the "mobility" of optimization algorithms, a distinction between *local* and *global* algorithms can be made. A local algorithm tends to converge to a local optimum of the objective function near the starting point. This is an uncritical behavior for functions with only one optimum within the search space. If the objective function has multiple stationary points where each defines a local optimum, a local algorithm might be unable to find the global optimum and converge to a local one. For such problems a global optimization algorithm is required. Figure 2.13 shows examples of objective functions representing a local and a global search problem. In general, deterministic algorithms mostly show local search behavior, whereas stochastic algorithms are suited for global search problems. To lower the number of required objective function evaluations, a hybrid algorithm can be applied. It uses a global algorithm to find a good starting point (near the global optimum) for the subsequently applied local algorithm. [25]

Concerning the number of dimensions of the objective space, optimization problems can be distinguished between *single-objective* and *multi-objective* problems. For the former a single scalar objective function exists that is subject to optimization. For the latter, multiple objective functions need to be simultaneously optimized. Accordingly, algorithms for both classes of problems exist. There are various ways a multi-objective

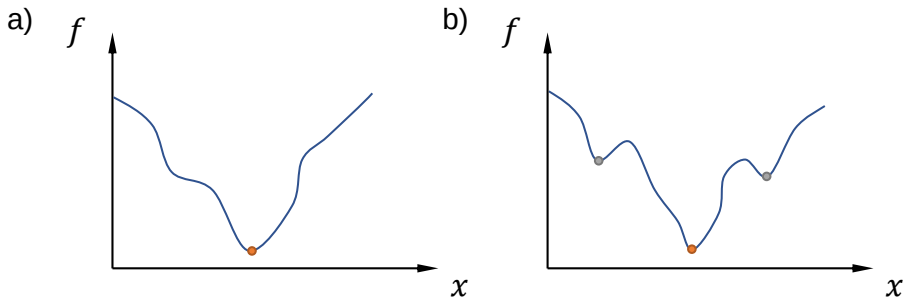

Figure 2.13: Examples of objective functions; a) single minimum, b) one global minimum and two local minima

problem can be solved. A very simple transformation of a multi-objective problem into a single-objective one can be done by the weighted-sum approach [9]

$$\bar{f} = \sum_{i=1}^{M} a_i \cdot f_i. \tag{2.4}$$

However, such an approach is biased as the weights a_i have to be defined a priori. There is no way to determine if only a slight change in weights might have resulted in a more favorable solution. A legit multi-objective optimization therefore always aims to find the so-called Pareto front of the optimization problem. The Pareto front, named after Italian engineer and economist Vilfredo Pareto, consists of all possible sets of optimization parameters that result in non-dominated objective values (Pareto dominance). Non-dominated in this context refers to solutions for which not a single objective value can be improved without worsening at least one of the others. Figure 2.14 shows an exemplary Pareto front for a minimization problem with two objectives. The region in the top right corner is suboptimal (dominated by the Pareto front) as improvements in one or both objectives are possible. The region in the bottom left corner is infeasible – for the defined search space and problem the objective function does not map to this area. The border in-between both regions represents the Pareto front that the optimization algorithm aims to find. [9]

Even within these categories many different algorithms exist. How well-suited a single algorithm is for solving a certain optimization problem not at least depends on the problem at hand. Listing, explaining and comparing different algorithms goes beyond the scope of this thesis and, as new algorithms are developed every year, would never be complete. The interested reader is referred to the literature, e.g. [25].

Another aspect shortly discussed at this point is *convergence*. The iterative nature of numerical optimization algorithms requires some sort of stopping criterion. In general, one is satisfied with the found approximated optimum if it is close enough to the actual optimum. As the actual optimum is of course unknown, this cannot serve as convergence criterion. Instead, other, less convenient criteria need to be applied, which many

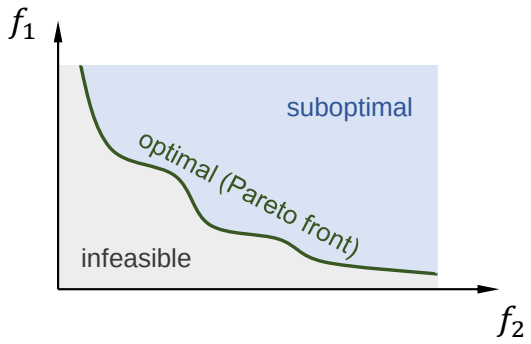

Figure 2.14: Exemplary Pareto front of a minimization problem with two objectives

times are algorithm-specific. However, especially for multi-objective optimizations some algorithm-independent metrics have been developed that allow an assessment of the optimization performance and progress. An overview is given in [36]. It should also be noted that for some algorithms general convergence is unproved and even disproved for special cases (including the Nelder-Mead method) [41].

2.4 Previous Research Regarding EV-Gearbox Designing

The application of optimization algorithms to perform the task of gearbox designing has been addressed in previous research work. In 2000, Chong and Lee [8] used a genetic algorithm to optimize the gearing parameters of a two-stage gear train. As the optimization of all gearing parameters leads to a high-dimensional search-space, their choice of a stochastic algorithm is still state of the art. Deterministic algorithms perform poorly on such problems and tend to converge to local optima. Furthermore, the design parameters of a gearbox require a mixed integer optimization (e.g. discrete number of teeth and real-valued face widths) for which the application of derivative-based methods is not sufficient [25].

The layout process of a gearbox for electric vehicles must consider multiple design objectives, such as minimizing costs as well as maximizing efficiency. Chong and Lee [8] and also the more recent work of Chandrasekaran et al. [7] treated the optimization problem as multi-objective. However, they used a weighted-sum-approach instead of the Pareto criterion. As pointed out before, although convenient this can be highly restrictive for the optimization and is insufficient for a holistic design method.

Regarding the system analysis process, most published work focusing on gearbox optimization make use of simplified calculation schemes for machine elements. This generally lowers the computational effort for the optimization – especially when using stochastic algorithms as mentioned before – but at the same time it seriously lowers the quality of the result. For a method that should provide a solid basis for design decisions in the early phases of the product development process, this is insufficient. The system analysis

model of a sophisticated and state-of-the-art design method as described in [30] must implement up-to-date calculation schemes based on current standards and guidelines, e.g. ISO 6336 for the load capacity calculation of the gears.

Another aspect that is rarely considered in published work is a holistic approach to the optimization problem. Gearing parameters only are optimized exemplary in [6], [7] and [8], omitting influences originating from the bearing selection, shafts, oil et cetera. However, a holistic design method must consider all relevant design goals as objectives and all design parameters that significantly influence these objectives as optimization parameters. In recent work, a holistic optimization approach for electrified powertrains is presented by Albers et al. [9] that focuses on battery, power electronics, electric motor and drivetrain. It outlines a general methodology on how the system interactions can be modeled. However, a specific design method and optimization strategy is not discussed there.

Concering the rating and optimization of the package integration of gearboxes (installation space demand compared to available installation space), mostly simplified metrics are applied and optimized in published work. Exemplary, an approximation of the gearbox volume is used by Sanghvi et al. in [37] and an approximation of the height of the gearbox by Altherr et al. in [5] – both also neglecting the available installation space, which might be provided as a requirement. However, the gearbox as well as the available installation space can show elaborate three-dimensional shapes that need to be taken into account in the package rating. Only then a sufficiently high level of detail is considered in a design method intended to provide a solid basis for design decisions.

3 Methodology

The following section presents one possible approach for a holistic design method for EV-gearboxes that overcomes the previously discussed limitations of existing methods (see section 2.4). The required system analysis models and the synthesizing strategy based on a multi-objective optimization are outlined, whereby the focus of the presented approach is set on the early phases of the product development process.

The formulation of the design problem regarding EV-gearboxes is schematically illustrated in Figure 3.1. Requirements, which are defined on system level "gearbox", serve as input to the design problem. The design task is now to find configurations of shafts, housing, gears, bearings et cetera, so that the resulting design fulfills all requirements. The components inside a gearbox interfere with each other with varying degrees (e.g. the gear wheel diameter affects the bearing reaction forces, the bearing diameter affects the required center distance of a gear pair and thus the gear wheel diameter). Finally, multiple gearbox solutions do exist in most cases and represent the output of the design process. A holistic approach needs to consider all of these possible designs. However, this might also include suboptimal designs, which are of no interest from an engineering point of view. Focusing only on Pareto-optimal solutions, the solution set is embodied by the Pareto front belonging to the design problem.

To achieve that, the presented design method iterates the phases of system analysis and design synthesis in a closed loop, as explained in section 2.2. A simplified structure of

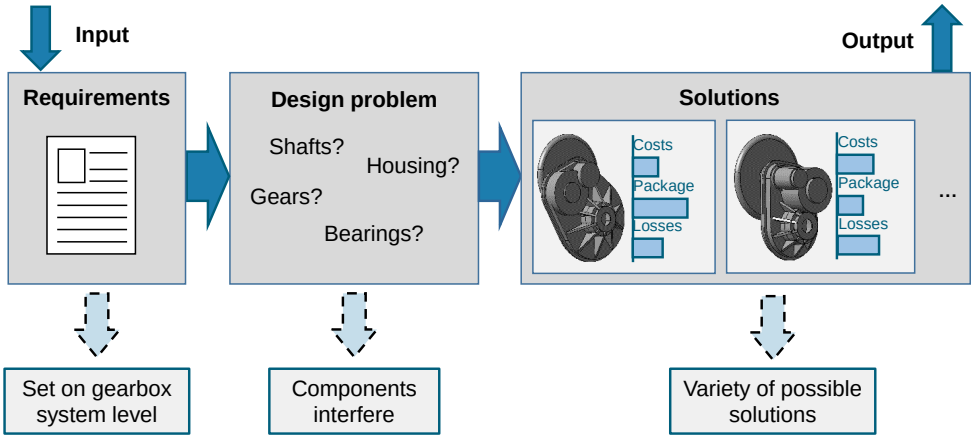

Figure 3.1: Schematic illustration of the design problem for EV-gearboxes

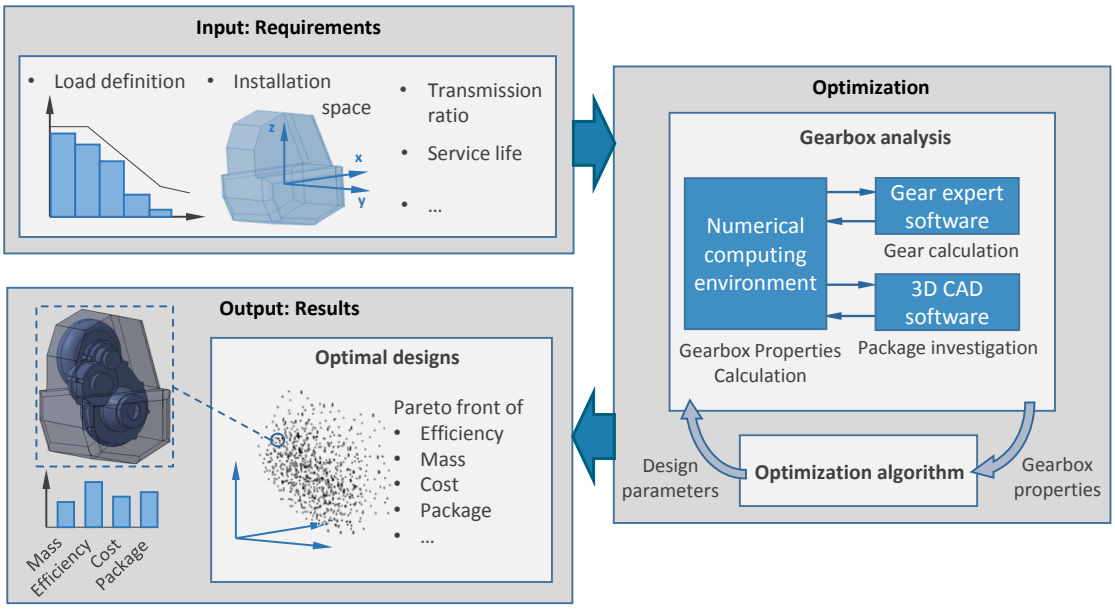

Figure 3.2: Illustration of the presented design process

the entire design process is shown in Figure 3.2. The synthesis at system level "gearbox" is performed by the optimization algorithm and thus fully automated. The optimization algorithm suggests design parameters, the analysis model evaluates the properties of the corresponding gearboxes and these are then passed to the optimization algorithm again. Based on the properties, new suggestions for the design parameters are made. This loop continues until converging behavior is observed.

The main requirements serving as input are

a) a load spectrum combined with a required service life based on which the load capacity of the machine elements is determined,

b) a driving cycle combined with vehicle data to calculate the power loss characteristics,

c) the total transmission ratio including a certain tolerance,

d) the available installation space in which the gearbox or entire e-drive should fit,

e) constraints related to the NVH-behavior (transverse contact ratio, overlap ratio and profile of the gears),

f) the maximum rotational speed of the electric machine (affecting the bearings concerning their limiting speeds) and

g) limits to the total center distance of the gearbox.

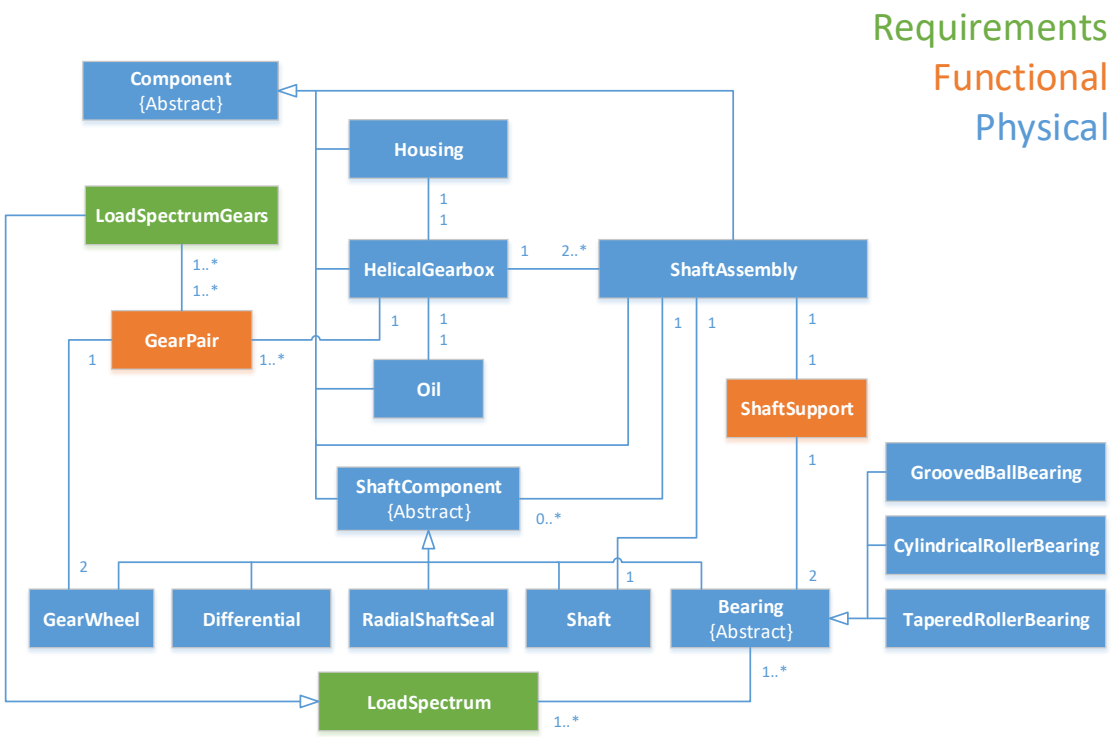

Figure 3.3: Class diagram of the gearbox analysis model

3.1 Gearbox Analysis Model

The required analysis model for the gearbox is explained in this section in greater detail. An advancement compared to the earlier published findings [16] has been made by generalizing and refining the entire model based on an object-oriented approach [32]. Moreover, the class structure of the model implementation follows the concept of ”Requirements, Functional, Logical, Physical” (RFLP) from model-based systems engineering [17]. The class diagram of the analysis model is shown in Figure 3.3 and gives an overview of the modeled gearbox components.

The top-level system ”gearbox” is represented by the class ”HelicalGearbox”. It is able to portray single-speed, multi-stage, helical gearboxes in offset or coaxial arrangements – especially motivated by the fact that such gearboxes with two-stages and offset output shaft represent the most common topology (see section 2.1). Assigned to each gearbox is a housing and a certain oil. Furthermore, an arbitrary number greater than or equal to two of shaft assemblies needs to be defined for the gearbox – all of them connected by single gear pairs. Each shaft assembly can contain an arbitrary number of shaft components and has a shaft support. Implemented as shaft components are gear wheels, differentials, radial shaft seals, shafts and rolling bearings. However, this list is extensible.

For evaluating the gearbox properties, various models and calculation schemes for all

components are required. These are outlined in the following sections. Mainly investigated are the load capacity, power losses, mass, costs and package characteristics of the gearbox system. Not investigated are subsystems like the lubrication and cooling system, a potential park lock integration, thermal interference with the electric machine and detailed NVH-characteristics – in the early product development phase the required data is mostly unavailable to include these aspects.

3.1.1 Load Definition

In general, the gearbox-internal loads change for different operating points. This implies that these loads have to be determined for every single operating point e.g. in a driving cycle. Exemplary, the Worldwide Harmonized Light Vehicles Test Cycle (WLTC) [42] for a class 3 vehicle contains up to 2 066 sample points – each corresponding to a certain operating point of the gearbox. Determining the gearbox-internal loads for all of these points comes with computational effort.

However, all (assumed) static forces and torques acting in a gearbox (e.g. torque transmitted by the single shafts, gear and bearing reaction forces) typically are linear dependent (friction neglected). By specifying one reference load L_{ref} at a certain location in the gearbox, the entire gearbox-internal load situation is defined. Due to this linear nature, unit loads $F_{\mathrm{u}\,i,j}$ and $T_{\mathrm{u}\,i,j}$ can be introduced for every force and torque at location i inside the gearbox. The index j denotes the load scenario, which will be explained later (see Figure 3.4). By multiplying these unit loads with the reference load, the corresponding forces and torques are obtained:

$$F_{i,j} = F_{\mathrm{u}\,i,j} \cdot L_{\mathrm{ref}\,j}, \tag{3.1}$$

$$T_{i,j} = T_{\mathrm{u}\,i,j} \cdot L_{\mathrm{ref}\,j}. \tag{3.2}$$

The gearbox-internal load situation now has to be solved only once for the unit loads. By simply scaling these with the reference load corresponding to a certain operating point, the actual acting forces and torques are acquired.

The implemented analysis model consistently uses the gearbox input torque T_{in} as reference load

$$L_{\mathrm{ref}\,j} = T_{\mathrm{in}}, \tag{3.3}$$

which makes most sense as the input torque is a known quantity imposed by the electric machine. However, for special load scenarios (e.g. park lock engagement) other reference loads might be more reasonable. Furthermore, the approach by equations (3.1) and (3.2) is only directly applicable if the sign of the input torque does not change. This is due to the fact that the radial gear forces do not change their sign when the torque direction is reversed – they always point to the center of the shaft. That way, the unit loads $F_{\mathrm{u}\,i,j}$

and $T_{\mathrm{u}\,i,j}$ are composed of two components (one for positive and one for negative sign of the reference load) and the distinction

$$F_{\mathrm{u}\,i,j} = \begin{cases} F_{\mathrm{u+}\,i,j} & \text{if } L_{\mathrm{ref}\,j} > 0 \\ F_{\mathrm{u-}\,i,j} & \text{otherwise} \end{cases}, \tag{3.4}$$

$$T_{\mathrm{u}\,i,j} = \begin{cases} T_{\mathrm{u+}\,i,j} & \text{if } L_{\mathrm{ref}\,j} > 0 \\ T_{\mathrm{u-}\,i,j} & \text{otherwise} \end{cases} \tag{3.5}$$

has to be made. The gearbox-internal load situation is thus fully described by a total of four different unit loads for each location, load scenario and an arbitrary gearbox input torque (e.g. originating from a load spectrum or a driving cycle). The unit loads are determined according to section 3.1.2.

A load scenario, in the context of this thesis, is defined by the unit loads in equations (3.4) and (3.5) together with a reference load L_{ref}. This means all gearbox-internal loads are linear dependent (described by the unit loads) for a certain load scenario. However, the unit loads across all load scenarios can differ – meaning arbitrary loads, for which the linear dependence described by equations (3.1) and (3.2) is no longer fulfilled, can be considered.

Exemplary, two load scenarios can be defined for a two-speed gearbox. The first scenario represents the load path inside the gearbox for driving in the first gear. The second scenario accordingly represents the load situation for driving in the second gear. As the load path changes when the gear is changed, separate unit loads have to be defined for each gear. The load situation is thus fully described by two load scenarios incorporating a total of eight unit loads for every location i inside the gearbox. Another example demonstrating the usefulness of load scenarios is the consideration of a park lock engagement when the vehicle is still moving at low velocity. This misuse case again shows a different load path inside the gearbox (depending on where the park lock is mounted) compared to regular driving. A load definition consisting of a load scenario for regular driving in the first gear, one for regular driving in the second gear and a park lock misuse case is illustrated in Figure 3.4.

The presented load definition consisting of load scenarios with corresponding reference and unit loads thus represents a very flexible approach – from only considering one load path for regular driving to highly non-linear cases where each operating point is described by a separate load scenario. For the former, computational benefits arise as solving the gearbox-internal load situation has to only be done for the unit loads – the used load definition is tailored for this. For the latter, all gearbox-internal loads are defined separately for each operating point. However, this hardly has any relevance for gearboxes (e.g. the total transmission ratio of a single-speed gearbox is constant, meaning the input torque is proportional to the output torque).

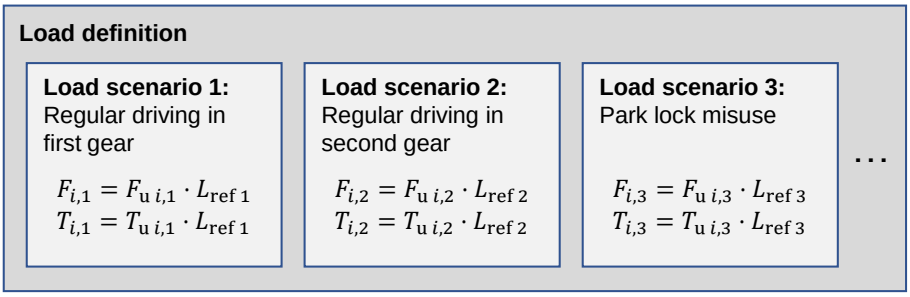

Figure 3.4: Exemplary illustration of a load definition based on various load scenarios

3.1.2 Gearbox-Internal Loads

How the forces and torques that are acting inside the gearbox can be calculated is presented in the following section. In particular, the (assumed) static bearing reaction forces and torques acting on the gear pairs need to be determined for the load capacity calculations described in section 3.1.3 and the gearbox losses in section 3.1.4. Rigid bearings, shafts and housing are assumed, meaning only two bearings per shaft can be applied. Otherwise the shaft support is statically over-determined, which requires the application of elastostatics for solving. For reasons of clarity, instead of the unit loads discussed in section 3.1.1 the absolute forces and torques are used in the following. However, the absolute loads can simply be substituted by the unit loads in the subsequent equations.

Gear Forces

The torque acting on gear wheel 1 of each gear pair inside a gearbox can easily be calculated from the single transmission ratios i_{GP}. Moving down the gear train starting at the input shaft, gear wheel 1 is always the first of the two wheels of a gear pair. In Figure 2.8 this would be the pinion on the input and intermediate shaft. Frictional forces and torques are neglected at this point. For a gearbox with n_{GP} gear pairs, the torque acting on the gear wheel at the input shaft is

$$T_{\mathrm{GP}\,1} = T_{\mathrm{in}}, \tag{3.6}$$

which is imposed by the electric machine. For all following gear pairs the acting torque on wheel 1 is

$$T_{\mathrm{GP}\,i} = T_{GP\,i-1} \cdot i_{\mathrm{GP}\,i-1},\ i \in [2, n_{\mathrm{GP}}]\,. \tag{3.7}$$

The gearbox output torque is then

$$T_{\mathrm{out}} = T_{\mathrm{GP}\,n_{\mathrm{GP}}} \cdot i_{\mathrm{GP}\,n_{\mathrm{GP}}} = T_{\mathrm{in}} \cdot i_{\mathrm{tot}}. \tag{3.8}$$

As the input torque for all gear pairs is now known, the corresponding tangential, radial and axial gear forces (F_{Wt}, F_{Wr} and F_{Wa}, respectively) acting at the pitch point can be determined. According to [24]

$$F_{\mathrm{Wt}} = \frac{2 \cdot T_{\mathrm{GP}}}{d_{\mathrm{W}}}, \tag{3.9}$$

$$F_{\mathrm{Wr}} = F_{\mathrm{Wt}} \cdot \tan(\alpha_{\mathrm{Wt}}), \tag{3.10}$$

$$F_{\mathrm{Wa}} = F_{\mathrm{Wt}} \cdot \tan(\beta_{\mathrm{W}}) \tag{3.11}$$

applies, where d_{W} is the pitch diameter of gear wheel 1, α_{Wt} denotes the operating pressure angle in the transverse plane and β_{W} is the helix angle at the pitch diameter. The directions in which these forces act on a shaft assembly are defined by the arrangement angles Θ_{SA} between the single shaft assemblies. The Cartesian coordinate system of an arbitrary shaft assembly inside a gearbox is chosen so that y denotes the axial direction and x and z lie in the radial plane as illustrated by Figures 3.5 and 3.6. Furthermore, the z-axis is aligned so that it crosses the center of the next shaft. That way, the gear forces originating from the gear pair connecting the next shaft i are already pointing in the x-, y- and z-direction of the currently investigated shaft assembly. The axial force of the previous gear pair $i-1$ as well already points in the y-direction of the shaft assembly coordinate system. However, the tangential and radial forces have to be broken up into their x- and z-components. With respect to Figure 3.5, this is achieved by

$$F_{\mathrm{Wrx}\,i-1} = F_{\mathrm{Wr}\,i-1} \cdot \sin(\overline{\Theta}_i) = -F_{\mathrm{Wr}\,i-1} \cdot \sin(\Theta_{\mathrm{SA}\,i}), \tag{3.12}$$

$$F_{\mathrm{Wrz}\,i-1} = -F_{\mathrm{Wr}\,i-1} \cdot \cos(\overline{\Theta}_i) = -F_{\mathrm{Wr}\,i-1} \cdot \cos(\Theta_{\mathrm{SA}\,i}), \tag{3.13}$$

$$F_{\mathrm{Wtx}\,i-1} = -F_{\mathrm{Wt}\,i-1} \cdot \cos(\overline{\Theta}_i) = -F_{\mathrm{Wt}\,i-1} \cdot \cos(\Theta_{\mathrm{SA}\,i}), \tag{3.14}$$

$$F_{\mathrm{Wtz}\,i-1} = -F_{\mathrm{Wt}\,i-1} \cdot \sin(\overline{\Theta}_i) = F_{\mathrm{Wt}\,i-1} \cdot \sin(\Theta_{\mathrm{SA}\,i}). \tag{3.15}$$

The total forces in x and z imposed by the previous gear pair on shaft assembly i are thus

$$F_{\mathrm{Wx}\,i-1} = F_{\mathrm{Wrx}\,i-1} + F_{\mathrm{Wtx}\,i-1} = -F_{\mathrm{Wr}\,i-1} \cdot \sin(\Theta_{\mathrm{SA}\,i}) - F_{\mathrm{Wt}\,i-1} \cdot \cos(\Theta_{\mathrm{SA}\,i}), \tag{3.16}$$

$$F_{\mathrm{Wz}\,i-1} = F_{\mathrm{Wrz}\,i-1} + F_{\mathrm{Wtz}\,i-1} = -F_{\mathrm{Wr}\,i-1} \cdot \cos(\Theta_{\mathrm{SA}\,i}) + F_{\mathrm{Wt}\,i-1} \cdot \sin(\Theta_{\mathrm{SA}\,i}) \tag{3.17}$$

and the total forces of the next gear pair are

$$F_{\mathrm{Wx}\,i} = -F_{\mathrm{Wt}\,i}, \tag{3.18}$$

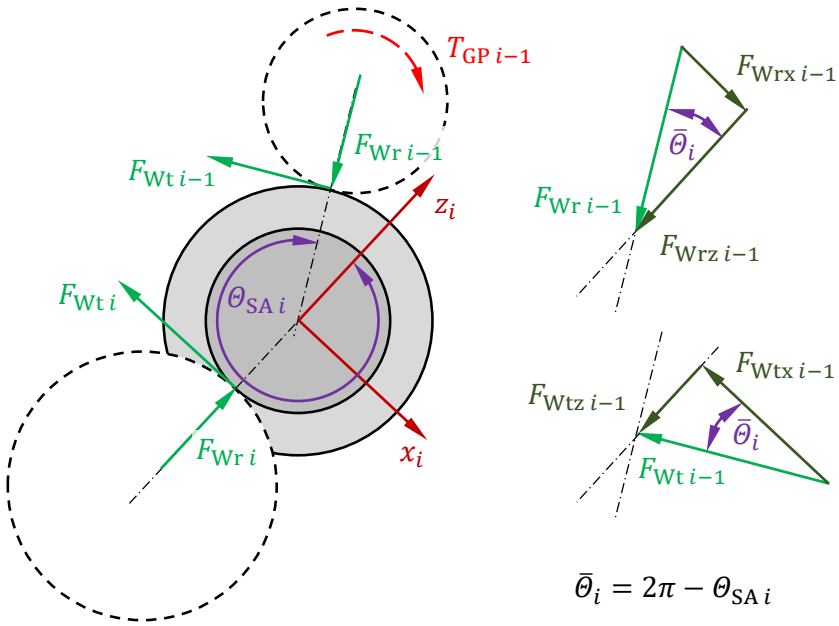

Figure 3.5: Gear forces acting on an arbitrary shaft assembly

$$F_{Wz\,i} = F_{Wr\,i}. \tag{3.19}$$

The position of the single pitch points in the shaft assembly coordinate system can also be determined with respect to Figure 3.5 (the drawn circles are the pitch circles). With the pitch diameters d_W of the single gear pairs the locations of the pitch points are

$$x_{W\,i-1} = -\frac{d_{W\,i-1}}{2} \cdot \sin(\overline{\Theta}) = \frac{d_{W\,i-1}}{2} \cdot \sin(\Theta_{SA\,i}), \tag{3.20}$$

$$z_{W\,i-1} = \frac{d_{W\,i-1}}{2} \cdot \cos(\overline{\Theta}) = \frac{d_{W\,i-1}}{2} \cdot \cos(\Theta_{SA\,i}), \tag{3.21}$$

$$x_{W\,i} = 0, \tag{3.22}$$

$$z_{W\,i} = -\frac{d_{W\,i}}{2}. \tag{3.23}$$

At this point it should be noted that the required gear geometry is calculated according to [24] and [26], which both use schemes based on the industry standard DIN 3960 [10].

Bearing Reaction Forces

In order to determine the bearing reaction forces, all acting forces on the shaft assembly induced by other shaft components have to be known. In fact, each shaft component can induce an arbitrary number of forces where each force is defined by its components

in x, y and z and the coordinates of its point of application. Equations (3.16) to (3.23) define these values for gear wheels. In general, not only forces but also torques might be imposed. However, for a gearbox this is only relevant at the input shaft (electric machine), covered by equation (3.6), and the output shaft (drive shafts), covered by equation (3.8).

Figure 3.6 shows a free-body diagram of a shaft assembly with two gear wheels that are imposing forces. Based on this illustration the required equations for calculating the bearing reaction forces for an arbitrary number of applied forces are derived. The conservation of momentum dictates that the sum of all forces and moments must be zero in the static case. For an arbitrary number n_F of action forces F this yields

$$F_{\mathrm{Bx}\,1} + F_{\mathrm{Bx}\,2} + \sum_{i=1}^{n_\mathrm{F}} F_{x\,i} = 0, \tag{3.24}$$

$$F_{\mathrm{By}\,1} + F_{\mathrm{By}\,2} + \sum_{i=1}^{n_\mathrm{F}} F_{y\,i} = 0, \tag{3.25}$$

$$F_{\mathrm{Bz}\,1} + F_{\mathrm{Bz}\,2} + \sum_{i=1}^{n_\mathrm{F}} F_{z\,i} = 0. \tag{3.26}$$

Furthermore, for the moment of all forces around the x-, y- and z-axis

$$F_{\mathrm{Bz}\,1} \cdot y_{\mathrm{BL}\,1} + F_{\mathrm{Bz}\,2} \cdot y_{\mathrm{BL}\,2} + \sum_{i=1}^{n_\mathrm{F}} F_{z\,i} \cdot y_{\mathrm{L}\,i} - \sum_{i=1}^{n_\mathrm{F}} F_{y\,i} \cdot z_{\mathrm{L}\,i} = 0, \tag{3.27}$$

$$T_\mathrm{shaft} + \sum_{i=1}^{n_\mathrm{F}} F_{x\,i} \cdot z_{\mathrm{L}\,i} - \sum_{i=1}^{n_\mathrm{F}} F_{z\,i} \cdot x_{\mathrm{L}\,i} = 0, \tag{3.28}$$

$$F_{\mathrm{Bx}\,1} \cdot y_{\mathrm{BL}\,1} + F_{\mathrm{Bx}\,2} \cdot y_{\mathrm{BL}\,2} + \sum_{i=1}^{n_\mathrm{F}} F_{x\,i} \cdot y_{\mathrm{L}\,i} - \sum_{i=1}^{n_\mathrm{F}} F_{y\,i} \cdot x_{\mathrm{L}\,i} = 0 \tag{3.29}$$

applies, where x_L, y_L and z_L define the position of the load application point of the corresponding force. The torque T_shaft is the sum of all axially induced torques on the shaft (e.g. driving torque of the electric machine on the input shaft). The location of the application point of the bearing reaction force defined by y_BL might be off-center from the actual bearing to account for the contact angle (e.g. tapered roller bearings).

The total axial bearing reaction force is

$$F_\mathrm{ByTot} = F_{\mathrm{By}\,1} + F_{\mathrm{By}\,2}. \tag{3.30}$$

How this axial force is distributed between both bearings depends on the type of bearing arrangement applied. For a locating/non-locating arrangement the locating bearing

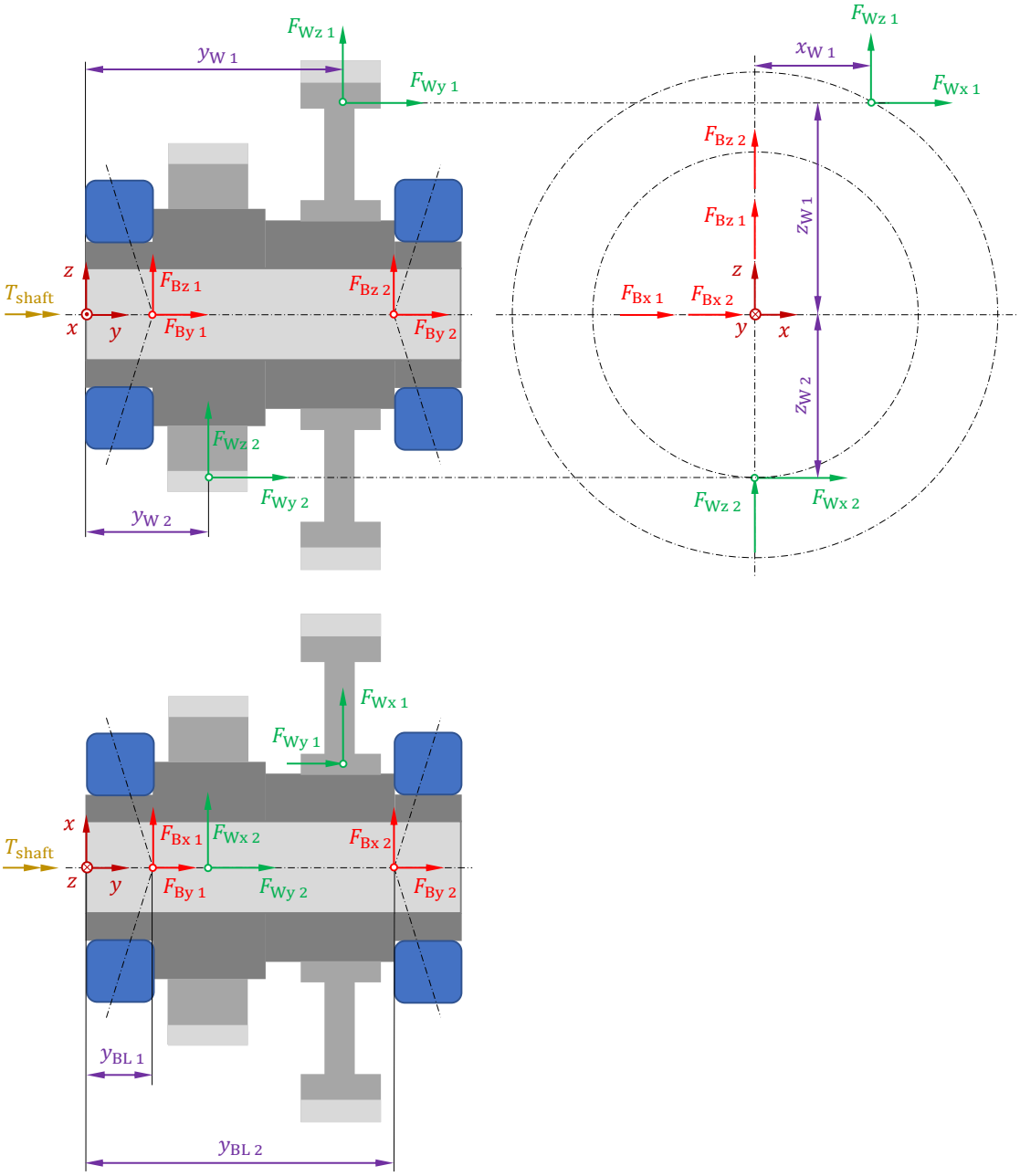

Figure 3.6: Free-body diagram of a shaft assembly with forces imposed by two gear wheels

supports the entire axial load. For an adjusted arrangement the direction of F_{ByTot} determines which bearing supports the load. However, for angular contact bearings (e.g. tapered roller bearings) an additional axial force has to be considered – due to the contact angle, a radial force will always induce an axial force. In that case F_{ByTot} is distributed according to the bearing manufacturer scheme [3]. Bearing preload forces are not considered.

With equations (3.25) and (3.30) the axial bearing reaction force is determined by

$$F_{\mathrm{ByTot}} = -\sum_{i=1}^{n_{\mathrm{F}}} F_{y\,i}. \tag{3.31}$$

The forces at bearing 1 (see Figure 3.6) in the radial plane are obtained from equations (3.24) and (3.26):

$$F_{\mathrm{Bx\,1}} = -F_{\mathrm{Bx\,2}} - \sum_{i=1}^{n_{\mathrm{F}}} F_{x\,i}, \tag{3.32}$$

$$F_{\mathrm{Bz\,1}} = -F_{\mathrm{Bz\,2}} - \sum_{i=1}^{n_{\mathrm{F}}} F_{z\,i}. \tag{3.33}$$

The corresponding forces at bearing 2 obtained by inserting equations (3.32) and (3.33) into equations (3.29) and (3.27) are

$$F_{\mathrm{Bx\,2}} = \frac{1}{y_{\mathrm{BL\,2}} - y_{\mathrm{BL\,1}}} \cdot \left(y_{\mathrm{BL\,1}} \cdot \sum_{i=1}^{n_{\mathrm{F}}} F_{x\,i} - \sum_{i=1}^{n_{\mathrm{F}}} F_{x\,i} \cdot y_{\mathrm{L}\,i} + \sum_{i=1}^{n_{\mathrm{F}}} F_{y\,i} \cdot x_{\mathrm{L}\,i} \right), \tag{3.34}$$

$$F_{\mathrm{Bz\,2}} = \frac{1}{y_{\mathrm{BL\,2}} - y_{\mathrm{BL\,1}}} \cdot \left(y_{\mathrm{BL\,1}} \cdot \sum_{i=1}^{n_{\mathrm{F}}} F_{z\,i} - \sum_{i=1}^{n_{\mathrm{F}}} F_{z\,i} \cdot y_{\mathrm{L}\,i} + \sum_{i=1}^{n_{\mathrm{F}}} F_{y\,i} \cdot z_{\mathrm{L}\,i} \right). \tag{3.35}$$

Equation (3.28) is not required for the computation of the bearing reaction forces but still has to be fulfilled. That way, it is implemented to identify any incorrectly set action forces leading to a total moment around the y-axis unequal to zero.

The vector addition of the orthogonal components F_{Bx} and F_{Bz} yields the radial bearing reaction force required for the load capacity and friction torque calculation:

$$F_{\mathrm{Br}} = \sqrt{F_{\mathrm{Bx}}^2 + F_{\mathrm{Bz}}^2}. \tag{3.36}$$

The presented calculation scheme has to be applied for all shaft assemblies inside the gearbox. Then all relevant torques and forces are determined for the subsequent evaluations.

3.1.3 Load Capacity

Based on the identified gearbox-internal loads, the capacity of the single machine elements inside the gearbox to withstand these loads can be determined. In particular, the shafts, gear wheels and bearings have to be examined. The relevant load is defined by a load spectrum consisting of multiple bins, where each bin is defined by a certain gearbox input or output torque, corresponding angular velocity and time slice (defining the number of load cycles in combination with the angular velocity). If the load spectrum is not directly given as a requirement, a two-parameter counting method is required to obtain it from measurements or simulation results. Exemplary, time-at-level counting or level-distribution counting might be applied. An overview of counting methods is given in [22].

Gear Wheels

The gear wheels are examined concerning tooth root bending fatigue and pitting. For that purpose, the implemented analysis model intercommunicates with a gear expert software [18]. That way, various calculation schemes can be applied – e.g. based on the industry standards DIN 3990 or ISO 6336. The risk for pitting is described by a safety factor based on the contact stress (Hertzian pressure) and the amount of tooth root bending fatigue by a safety factor based on the maximum tensile stress at the root. The contact stress according to ISO 6336 [20] is defined by

$$\sigma_{\mathrm{H}} = Z_{\mathrm{H}} Z_{\mathrm{E}} Z_{\varepsilon} Z_{\beta} \sqrt{\frac{|F_{\mathrm{t}}|}{d\,b} \frac{u+1}{u} K_{\mathrm{A}} K_{\mathrm{V}} K_{\mathrm{H}\beta} K_{\mathrm{H}\alpha}}, \tag{3.37}$$

where the tangential force at the reference diameter is

$$F_{\mathrm{t}} = \frac{2 \cdot T_{\mathrm{GP}}}{d} \tag{3.38}$$

and d denotes the reference diameter of gear wheel 1 (compare to equation (3.9)) [26]. The other influencing quantities are

- the zone factor Z_{H}, considering the flank curvatures at the pitch point and transforming the tangential load at the reference diameter to the tangential load at the pitch diameter,
- the elasticity factor Z_{E}, considering the elastic properties of the gear wheel materials,
- the contact ratio factor Z_{ε}, considering the effective length of the lines of contact,
- the helix angle factor for contact stress Z_{β}, considering influences of the helix angle, such as the variation of the load along the lines of contact,

- the face width b,
- the tooth ratio $u = z_2/z_1$, where z_2 denotes the number of teeth of gear wheel 2 and z_1 the number of teeth of gear wheel 1,
- the application factor K_{A}, considering uncertainties in the load assumptions,
- the dynamic factor K_{V}, considering internal dynamic effects on the load (meshing of the gear pair),
- the face load factor for contact stress $K_{\mathrm{H}\beta}$, considering the uneven load distribution over the face width (e.g. due to mesh misalignment caused by manufacturing tolerances, elastic deformations et cetera) and
- the transverse load factor for contact stress $K_{\mathrm{H}\alpha}$, considering the uneven load distribution in the transverse direction (e.g. due to pitch deviations resulting from manufacturing tolerances).

Analogously, the tensile stress at the tooth root due to bending is

$$\sigma_{\mathrm{F}} = \frac{|F_{\mathrm{t}}|}{b\, m_{\mathrm{n}}} Y_{\mathrm{F}} Y_{\mathrm{S}} Y_{\beta} Y_{\mathrm{B}} Y_{\mathrm{DT}} K_{\mathrm{A}} K_{\mathrm{v}} K_{\mathrm{F}\beta} K_{\mathrm{F}\alpha}. \tag{3.39}$$

The so far undescribed influences are

- the normal module m_{n},
- the tooth form factor Y_{F}, considering the influence of the tooth form on the nominal tooth root stress,
- the stress correction factor Y_{S}, considering the relation between nominal and actual tooth root stress,
- the helix angle factor for tooth root stress Y_{β}, considering the fact that the bending moment at the tooth root of helical gears is smaller than for the corresponding virtual spur gears,
- the rim thickness factor Y_{B}, considering the influence of the rim thickness on the tooth root stresses,
- the deep tooth factor Y_{DT}, which adjusts the calculated tooth root stress for high precision gears,
- the face load factor for tooth root stress $K_{\mathrm{F}\beta}$, considering the uneven load distribution over the face width (e.g. due to mesh misalignment caused by manufacturing tolerances, elastic deformations et cetera) and
- the transverse load factor for tooth root stress $K_{\mathrm{F}\alpha}$, considering the uneven load distribution in the transverse direction (e.g. due to pitch deviations resulting from manufacturing tolerances).

To address the varying load conditions defined by the load spectrum, these stresses have to be calculated for all bins of the load spectrum. Depending on the number of load cycles n_{LC} in each bin, the corresponding stresses cause a certain amount of damage to the material. The damage accumulation for the entire spectrum can be calculated according to the Palmgren-Miner rule [20]

$$U = \sum_{i=1}^{n_{\mathrm{LB}}} \frac{n_{\mathrm{LC}\,i}}{n_{\mathrm{LC\,lim}\,i}}, \tag{3.40}$$

where n_{LB} denotes the number of bins in the load spectrum and $n_{\mathrm{LC\,lim}}$ is the maximum number of load cycles before failure occurs corresponding to the calculated stresses. It is obtained from the stress-cycle curve of the material. Failure due to fatigue can be expected when this damage sum becomes greater than one. The limiting case is thus described by

$$\sum_{i=1}^{n_{\mathrm{LB}}} \frac{n_{\mathrm{LC}\,i}}{n_{\mathrm{LC\,lim}\,i}} = 1. \tag{3.41}$$

The actual safety factors $S = \{S_{\mathrm{H}}, S_{\mathrm{F}}\}$ are incorporated in the maximum permissible stress by shifting the stress-cycle curve. Depending on the shape of this curve, the relation between stress and maximum number of load cycles before failure $n_{\mathrm{LC\,lim}}\,(\sigma \cdot S)$ is defined, where $\sigma_{\mathrm{H}} \cdot S_{\mathrm{H}}$ is to be used for the pitting calculation and $\sigma_{\mathrm{F}} \cdot S_{\mathrm{F}}$ for the tooth root fatigue calculation. The actual relations can be found in ISO 6336-6 [20]. In order to determine the safety factors, an iterative approach has to be chosen. Starting from unity values, the safety factors are adjusted until equation (3.41) is fulfilled (with sufficient precision). When the so determined safety factors are equal to or greater than one, according to this scheme the gear wheels will withstand the imposed load. [20]

Other damage mechanisms besides pitting and tooth root bending fatigue are not investigated. However, plastic yielding might be of interest when a potential park lock is engaged (especially in the misuse case) or fast powertrain decelerations occur, e.g. induced by a wheel brakes application of the vehicle dynamics control.

Bearings

The bearings are examined concerning their static load capacity (static load rating) and their fatigue lifetime (dynamic load rating). The static load capacity is relevant for cases in which the bearing is standing still or rotating at a small velocity. This is of relevance in e-drives due to the torque characteristic of the electric machine. Peak torques occur at low or even zero velocity when rapidly accelerating from a standstill – meaning peak bearing loads are present at low or zero velocity. The load capacity is evaluated according to [3] and [29], which both use schemes based on the industry standards DIN ISO 76 and ISO 281.

For the static load capacity a safety factor S_0 is determined according to

$$S_0 = \frac{C_{0\mathrm{r}}}{P_{0\mathrm{r}}}, \tag{3.42}$$

where $C_{0\mathrm{r}}$ is the static load rating of a radial bearing and the combined static radial load is

$$P_{0\mathrm{r}} = X_0 \cdot F_{\mathrm{Br}} + Y_0 \cdot |F_{\mathrm{By}}|. \tag{3.43}$$

The coefficients X_0 and Y_0 depend on the bearing type and geometry. The static safety factor S_0 needs to be evaluated for all bins of the load spectrum. The static load capacity of the bearing is sufficient when all determined safety factors are greater than a certain minimum value. Especially for roller bearings, this value is greater than one (1.5 for rotating operation in normal conditions). Suggestions for minimum values of S_0 are given in [29].

For the dynamic load capacity, again based on the Palmgren-Miner rule (equation (3.41)), equivalent operating conditions considering the load spectrum are determined first. The equivalent rotational velocity n_{eq} is determined from the time slice ratio q (e.g. operating hours in bin divided by total operating hours) and the rotational velocity of the bearing n_{B} in each bin of the load spectrum:

$$n_{\mathrm{eq}} = \sum_{i=1}^{n_{\mathrm{LB}}} q_i \cdot n_{\mathrm{B}\,i}. \tag{3.44}$$

The equivalent dynamic radial load is

$$P_{\mathrm{r\,eq}} = \sqrt[p]{\frac{\sum_{i=1}^{n_{\mathrm{LB}}} q_i \cdot n_{\mathrm{B}\,i} \cdot P_{\mathrm{r}\,i}^{p} / a_{\mathrm{ISO}\,i}}{n_{\mathrm{eq}}}}, \tag{3.45}$$

where p denotes the slope of the stress-cycle curve of the bearing (3 for ball bearings and 10/3 for roller bearings [3]). The combined dynamic radial load is analogous to equation (3.43)

$$P_{\mathrm{r}} = X \cdot F_{\mathrm{Br}} + Y \cdot |F_{\mathrm{By}}| \tag{3.46}$$

and a_{ISO} is the stress-lifetime modification factor. This factor takes a unity value for the nominal calculation scheme and a possibly smaller or greater value for the extended scheme. It accounts for various influences originating from the load, material, operating conditions and in particular the lubrication quality. This is of importance in gearboxes for e-drives, as requirements regarding efficiency lead to the application of oils with very low viscosity. The nominal calculation scheme neglects this aspect.

The fatigue lifetime of each bearing is then calculated by

$$L_{\mathrm{B}} = a_1 \cdot \frac{1}{n_{\mathrm{eq}}} \cdot \left(\frac{C_{\mathrm{r}}}{P_{\mathrm{r\,eq}}} \right)^p, \tag{3.47}$$

where a_1 is the failure probability factor. For a reliability probability of 90 % it takes a unity value. Only bearings with a fatigue lifetime equal to or greater than the service life set as a requirement for the gearbox and a sufficiently high static safety factor are eligible for the gearbox design.

Shafts

Contrary to the load capacity calculation of the gears and bearings, no detailed fatigue analysis of the shafts is performed. Typically, hollow shafts with a compact shape are found in gearboxes for e-drives (see Figure 2.8). Accordingly, no large lever arms of forces exist and thus no large bending moments compared to the cross-sectional second area moment are induced. In fact, a post-processing of the results of various case studies including the ones in section 4 revealed no critical fatigue at the shafts with the following approach.

Based on a nominal shaft torque T_{nom} and a permissible torsional stress τ_{p}, the required shaft diameters are determined. Assuming a known diameter ratio

$$Q_{\mathrm{D}} = \frac{d_{\mathrm{inner}}}{d_{\mathrm{outer}}}, \tag{3.48}$$

the minimum required outer diameter is obtained from

$$d_{\mathrm{outer}} = \sqrt[3]{\frac{16 \cdot T_{\mathrm{nom}}}{\pi \cdot \tau_{\mathrm{p}} \cdot \left(1 - Q_{\mathrm{D}}^4\right)}}. \tag{3.49}$$

The corresponding inner diameter is determined by rearranging equation (3.48) and is used as actual inner diameter in the design of the hollow shafts. The outer shaft diameter may not fall below the determined minimum shaft diameter at any point. Only then a shaft with a sufficiently high load capacity is present.

3.1.4 Frictional Losses

Until now, frictional forces and torques have been neglected since they are small compared to the operating load. However, requirements regarding efficiency are set for the gearbox system as input to the design method. For the implemented analysis model, gear wheels, bearings and radial shaft seals cause frictional torques during operation,

which lower the torque output of the gearbox and thus cause a power loss. In general, these losses should be as low as possible for an optimally designed gearbox.

A distinction can be made between load-dependent and velocity-dependent losses. The former are induced by normal forces in the moving contact regions of the single machine elements (e.g. gear tooth flanks, rolling elements and races of bearings). The latter are primarily induced by viscous forces depending on the oil viscosity and rotational speed. The degree of efficiency for a gearbox is defined as

$$\eta = 1 - \frac{P_\mathrm{l}}{P_\mathrm{in}} = 1 - \lambda, \tag{3.50}$$

where P_l is the sum of all power losses, P_in is the input power and λ is the degree of losses. It should be noted that the input power does not necessarily equal the power transmitted by the input shaft of the gearbox. During regenerative braking, the power flow direction is reversed in which case the input power is transmitted by the output shaft of the gearbox.

A time-averaged degree of efficiency for time-variant power losses $P_\mathrm{l}(t)$ and input power $P_\mathrm{in}(t)$ needs to be determined by integrating the lost and input power to obtain the respective lost and input energy according to

$$\overline{\eta} = 1 - \frac{\int_0^{t_\mathrm{end}} P_\mathrm{l}(t)\mathrm{d}t}{\int_0^{t_\mathrm{end}} P_\mathrm{in}(t)\mathrm{d}t} = 1 - \frac{W_\mathrm{l}}{W_\mathrm{in}} = 1 - \overline{\lambda}. \tag{3.51}$$

This is relevant for determining the degree of efficiency or losses e.g. based on a driving cycle, like the Worldwide Harmonized Light Vehicles Test Cycle (WLTC) [42].

Gear Wheels

The frictional power loss resulting from the meshing of a gear pair is determined according to [26]. The load-dependent loss is

$$P_{\mathrm{l\,GP\,L}} = P_{\mathrm{GP\,in}} \cdot \mu_\mathrm{mZ} \cdot H_\mathrm{V}, \tag{3.52}$$

where $P_{\mathrm{GP\,in}}$ denotes the input power for the gear pair, μ_mZ is the mean gear friction coefficient and H_V the gear power loss factor. H_V incorporates information of the gear geometry and is defined as

$$H_\mathrm{V} = \pi \left(\frac{1}{z_1} + \frac{1}{z_2} \right) \frac{1}{\cos\beta_\mathrm{b}} \left(1 + \varepsilon_1^2 + \varepsilon_2^2 - \varepsilon_\alpha \right), \tag{3.53}$$

where β_b is the helix angle at the base circle, ε_1 the contact ratio of the tooth tips, ε_2 the contact ratio of the tooth roots and ε_α the transverse contact ratio. The mean gear

friction coefficient μ_{mZ} takes a value of approximately 0.04 for mineral oils of the ISO viscosity classes VG 100 to 200 [26]. As the corresponding viscosities are rather high for gearboxes in e-drives, μ_{mZ} is determined according to the relations given in [26] (in particular equation (6.6/7), page 364).

The velocity-dependent losses $P_{\mathrm{l\,GP\,V}}$ are determined according to the applied lubrication type and empirical relations [26]. Implemented are losses for spray and splash lubrication, whereby the latter not only depend on the velocity but also the immersion depth of the gear wheel. The total power loss of a single gear pair is then given by

$$P_{\mathrm{l\,GP}} = P_{\mathrm{l\,GP\,L}} + P_{\mathrm{l\,GP\,V}}. \tag{3.54}$$

Bearings

The power loss occurring at the bearings is determined according to [29] and the bearing manufacturer scheme [3], both based on DIN ISO 15312. The load-dependent loss is

$$P_{\mathrm{l\,B\,L}} = n_{\mathrm{B}} \cdot f_1 \cdot P_1 \cdot d_{\mathrm{M}}, \tag{3.55}$$

where f_1 denotes the load-dependent friction coefficient according to the bearing type and size, d_{M} is the mean diameter of the bearing and P_1 the determining load. It is defined as

$$P_1 = X_1 \cdot F_{\mathrm{Br}} + Y_1 \cdot |F_{\mathrm{By}}|, \tag{3.56}$$

where the factors X_1 and Y_1 depend on the type of bearing (compare to equations (3.43) and (3.46)). The velocity-dependent power loss is

$$P_{\mathrm{l\,B\,V}} = \begin{cases} n_{\mathrm{B}} \cdot f_0 \cdot (\nu \cdot n_{\mathrm{B}})^{2/3} \cdot d_{\mathrm{M}}^3 & \text{if } \nu \cdot n_{\mathrm{B}} \geq 2000\,\frac{\mathrm{mm}^2}{\mathrm{s}}\frac{1}{\mathrm{min}} \\ n_{\mathrm{B}} \cdot f_0 \cdot 160\,\frac{\mathrm{mm}^2}{\mathrm{s}}\frac{1}{\mathrm{min}} \cdot d_{\mathrm{M}}^3 & \text{otherwise} \end{cases}, \tag{3.57}$$

where f_0 is the velocity-dependent friction coefficient, which is determined based on the bearing type, size and the lubrication type. The total bearing losses are then

$$P_{\mathrm{l\,B}} = P_{\mathrm{l\,B\,L}} + P_{\mathrm{l\,B\,V}}. \tag{3.58}$$

Radial Shaft Seals

Radial shaft seals are contact seals and thus induce a frictional loss when the shaft is rotating. In fact, many influences affect this frictional loss including the material used for the seal, the hardness of the material used for the shaft, the surface roughness of

the shaft in the region of the sealing lip, the lubricant used and the temperature at the sealing point. An empirical relation is given in [26] to determine the power loss, which is

$$P_{\mathrm{l\,RSS}} = [145 - 1.6 \cdot \vartheta_{\mathrm{oil}} + 350 \cdot \log(\log(\nu_{40} + 0.8))] \cdot d_{\mathrm{RSS}}^2 \cdot n \cdot 10^{-7}. \tag{3.59}$$

The oil temperature at the sealing point ϑ_{oil} needs to be inserted into equation (3.59) with unit °C, the nominal oil viscosity ν_{40} in mm^2/s, the shaft diameter at the sealing point d_{RSS} in mm and the rotational velocity of the shaft n in rpm. Equation (3.59) then yields the seal power loss in watt.

3.1.5 Mass & Costs

The determination of the mass and costs of the gearbox system is of high relevance as minimizing these quantities might be a design target (and thus an optimization objective). The mass and costs of the bearings, radial shaft seals and differentials are taken from databases. The mass of the shafts, gear wheels and the housing is obtained from an approximation of their volume and a specified density for the applied materials:

$$m = \rho \cdot V_{\mathrm{approx}}. \tag{3.60}$$

The shafts are assumed to consist of an arbitrary number of hollow segments with a certain inner and outer diameter as well as a segment length. The total volume of the shaft is determined by addition of all segment volumes (hollow cylinders).

In the most common case, the gear wheels are assumed to have the radial contour depicted in Figure 3.7. Rotating this contour around the y-axis by 2π yields the volume of the gear wheel. To account for the gaps in-between the single teeth, the outer diameter for the volume approximation is assumed to be the reference diameter d.

The approach for the volume calculation of the housing is illustrated in Figure 3.8. The single radial contours of the shaft assemblies are offset by a specified clearance between interior and housing. The openings in the housing at the input and output shaft on the left-hand or right-hand side are considered. This offset contour is then thickened by the specified housing thickness and revolved around the y-axis by 2π. The so determined partial volumes corresponding to all shaft assemblies are added together to obtain an approximation of the housing volume. Accordingly, in the overlapping regions of two partial volumes the volume is counted twice – this leads to a higher value for the approximated volume compared to the actual one. A more accurate alternative to the described 2D-method is to rely on a 3D-CAD model as discussed in the previous publication [16]. However, such an approach is hardly generalizable, comes with huge computational effort and possibly robustness issues for ill-defined models, making it unsuitable for the presented method.

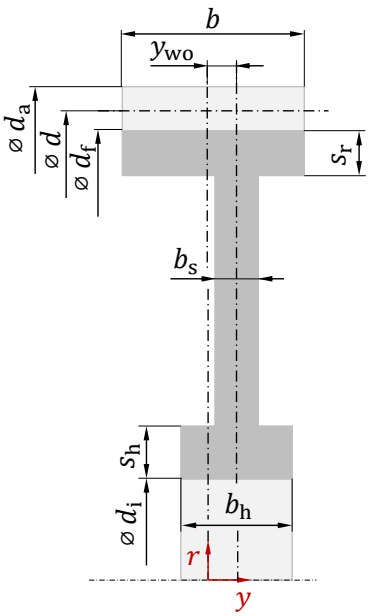

Figure 3.7: Most common shape of a gear wheel for the implemented analysis model

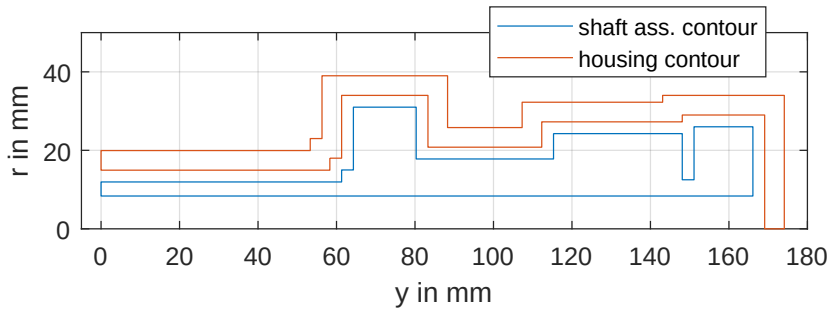

Figure 3.8: Approximation of the housing contour for an exemplary input shaft

The costs of the shafts, gear wheels and the housing are determined by a cost factor c and the mass of the single components:

$$C = c \cdot m. \tag{3.61}$$

For series production gearboxes and their components, this cost factor c can be identified from experience with sufficient accuracy [23].

Cost Degression by Applying a Common-Part Approach

It is a well-known fact that a reduction of the number of unique components inside a system in general lowers the costs. A common-part approach follows this logic to decrease the total costs and thus achieve advantages at the market. The number of common parts then increases resulting in a larger quantity demand for all single common parts. Ehrlenspiel et al. [12] describe five main influences on the cost degression by increasing the quantity, which are

a) degression of the one-off costs,
Each unique part has to be developed, requires a production planning and a corresponding production line and logistics strategy set up.

b) degression due to training effect,
A new working step requires training and becomes more familiar when repeated many times. For a smaller number of unique components, training shows less effort and is more efficient.

c) degression due to optimized designs,
As common parts reduce the number of unique components, more time can be spent designing these parts and optimizing them for minimum production and logistics costs.

d) degression due to more efficient production processes,
The quantity required of a single part directly influences the amount of acceptable investment costs for the production line. More efficient processes that reduce the production costs of a single part in general show higher one-off costs. However, as these costs are divided among all produced parts, large quantities justify efficient processes and are thus cheaper per part.

e) degression due to quantity discount.
A larger quantity of purchased parts and resources in general reduces the achievable purchasing prices at the market.

Not all of the listed influences might have the same relevance for gearboxes in e-drives. However, a comparable example is given in [12] for production costs of an automotive internal combustion engine, illustrated in Figure 3.9. With known reference costs C_0 and quantity n_{P0} the costs change according to

$$C = C_0 \cdot \frac{1}{\sqrt[3]{n_{\mathrm{P}}/n_{\mathrm{P0}}}}. \tag{3.62}$$

This means the costs are decreased by around 20 % when the quantity is doubled. As the cost degression due to quantity discounts can also be described by equation (3.62) according to [12], this can exemplary be applied to the bearings inside a gearbox – they are typically purchased parts. For a two-stage helical gearbox, as shown in Figure 2.8, a

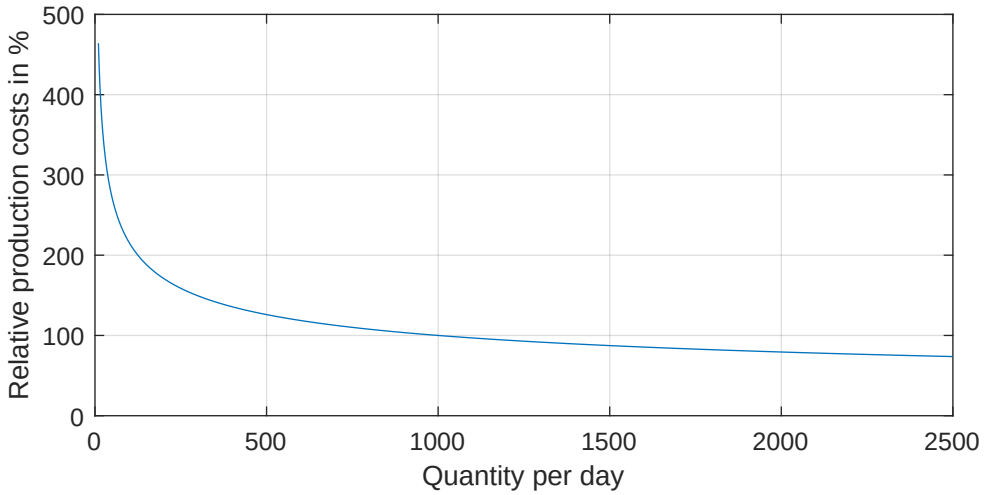

Figure 3.9: Exemplary cost degression by increasing the number of produced ICEs [12], curve according to equation (3.62)

maximum of six unique bearings and a minimum of only one unique bearing is eligible. The cost degression according to equation (3.62) between these two extreme cases is around 45 %. However, this only affects the bearing costs. The shafts, gears and housing might become more expensive when such a common-part approach is enforced for the bearings. Moreover, the package demand, the mass and the gearbox efficiency might take unacceptable values. A holistic design method has to consider all influences and only choose a common-part approach to an extend, which is favorable for the optimality of the entire gearbox system.

To include common-part aspects, two possible approaches arise:

a) minimization of the number of unique components (explicit) or

b) consideration of the cost degression (implicit).

The former is (as described above) a restrictive approach as the actual cost benefit is not directly apparent, but it also eliminates the necessity of a sophisticated cost model – the number of unique components is explicitly formulated as an optimization objective. The latter indeed requires a direct description of the cost benefits by the cost model – common-part aspects are implicitly considered by the cost model and do not require an additional optimization objective.

To allow for such an implicit approach, an arbitrary cost model taking the entire gearbox object as an input can be specified for the described analysis model. Thus, the determined costs represent the actual costs originating from the system context. It should be noted that this approach can be extended to not only consider gearbox designs for a single design problem but to also consider multiple concurrent design problems and already existing designs. This leads to the definition of a platform approach and thus a

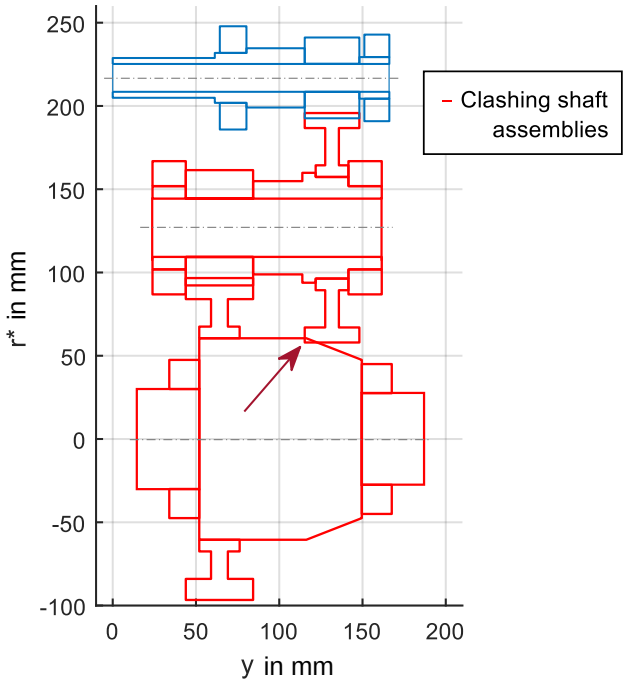

Figure 3.10: Clash of the radial contours of intermediate and output shaft

holistic cost model. However, this also drastically increases the complexity for the design method and needs to be addressed in future research work.

3.1.6 Validity Checks

Further analysis methods are required to identify invalid gearbox configurations. Exemplary, designs of the intermediate and output shaft might have been chosen so that a clash of the single shaft assemblies occurs. Such a situation is depicted in Figure 3.10, where the bull gear at the intermediate shaft clashes with the carrier of the differential at the output shaft. It should be noted that the radial coordinate direction r^* in Figure 3.10 represents the unwound radial projections – all shafts lie in a common plane for better visualization.

The strategy applied for detecting gearbox-internal clashes is described in the following. All components of a shaft assembly are assumed to be rotationally symmetric and thus have a radial contour. The contours of the single components are merged together considering their axial offsets to obtain radial contours for all shaft assemblies. Each shaft assembly is now tested against clashes with all other shaft assemblies by identifying polygon intersections of the radial contours. To do so, the contours of the currently tested pair of assemblies are offset by a certain safety clearance and at the bearings additionally by the required thickness of the bearing fits of the housing. They are then brought into

their proper relative arrangement considering their center distances and axial positions. That way, if any of the tested radial contours shows an intersection that is not due to the meshing of a connecting gear pair, a clashing situation is detected and the gearbox design identified as invalid. For a two-stage gearbox this means a clash detection of the input and intermediate shaft, the input and the output shaft as well as the intermediate and the output shaft has to be performed.

Again, a 3D-CAD model of the gearbox interior can be used to determine clashes instead of the presented 2D approach. However, besides the advantage that also shaft components which are not rotationally symmetric can be considered (e.g. accurate park lock geometry), this comes with the same disadvantages already discussed in section 3.1.5. Moreover, further situations leading to an invalid design need to be reliably detected by the analysis model (e.g. impermissible undercut at the gear wheels). All criteria distinguishing between valid and invalid configurations are implemented as constraints for the optimization and further discussed in section 3.3.1.3.

3.2 Package Analysis Model

For assessing the package situation, a suitable model is required that gives a quantitative statement based on which the package integration can be rated. As shortly discussed in section 2.3, simple metrics can be applied, which to some extend represent the installation space demand of the gearbox. Such simple metrics can be directly derived from the gearbox properties and do not require high computational efforts. For that reason the volume of the bounding box of the gearbox, its total extensions in all three spacial dimensions and a so-called ground clearance metric are implemented. The latter is defined by the tip diameter of the gear wheel at the output shaft – minimizing this metric will maximize the clearance between gearbox and roadway (in case the tip diameter defines the lowest point). Optimizing the installation space demand of the gearbox based on these metrics might be sufficient in some cases.

However, many times a conceptual vehicle design exists when approaching the task of powertrain designing and a 3D-CAD model of the available installation space is defined as input to the design task. Furthermore, this installation space is often intended to accommodate the entire e-drive and not only the gearbox. This means a legit analysis model has to consider a given installation space, the space demand by the power electronics unit, electric machine and gearbox as well as their arrangement. Investigating the resulting package situation is indeed complicated, which is why a package analysis based on a 3D-CAD model is chosen in the presented approach. For that purpose, the optimization process intercommunicates with a suitable CAD software [35].

The installation space demand of the power electronics unit is defined by an arbitrary solid body provided as input. The electric machine is represented by a parametric model consisting of a right circular cylinder with corresponding length and diameter. For the gearbox, the package model is defined by the outer geometry of the housing as explained

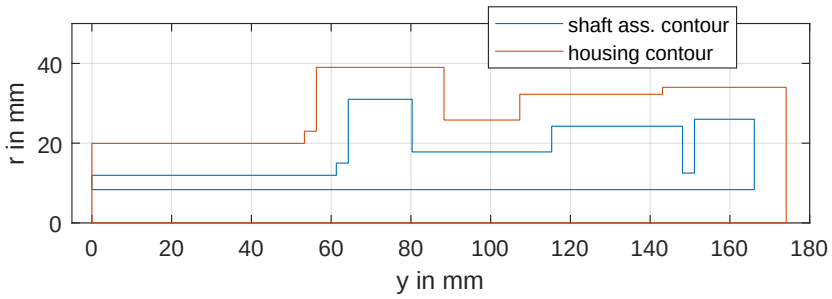

Figure 3.11: Radial package model contour for an exemplary input shaft

in section 3.1.5. However, the bodies of revolution are no longer hollow as indicated by the radial contour in Figure 3.11. The bodies of all shaft assemblies are brought into their proper spacial arrangement and merged by boolean operations. Thus, a single solid body is obtained representing the installation space demand of the gearbox.

All of the three components inside an e-drive can be arranged in various ways. The power electronics unit is assumed to be in a tangential arrangement with the electric machine. The implemented arrangement parameters are illustrated in Figure 3.12 and contain the

a) axial offset of the powertrain y_{PT},

b) tilt angle of the powertrain Θ_{PT},

c) axial offset of the power electronics unit to the front face of the electric machine y_{PE},

d) tangential offset of the power electronics unit t_{PE},

e) arrangement angle of the power electronics unit with respect to the installation space coordinate system Θ_{PE} and

f) a further boolean parameter describing in which direction the powertrain is facing (y_{PT0} and y_{IS0} pointing in the same or opponent direction).

The origin of the powertrain coordinate system lies on the y-axis of the installation space system, which is defined to be coincidental with the corresponding axle of the vehicle. Furthermore, the installation space requirements are provided by two solids representing the

a) available installation space and a

b) forbidden installation space.

The former defines the desired space in which the e-drive should fit. The latter defines regions with which intersections are impermissible. Exemplary, such a situation is present when the power electronics unit intersects the drive shafts or the e-drive or is tilted

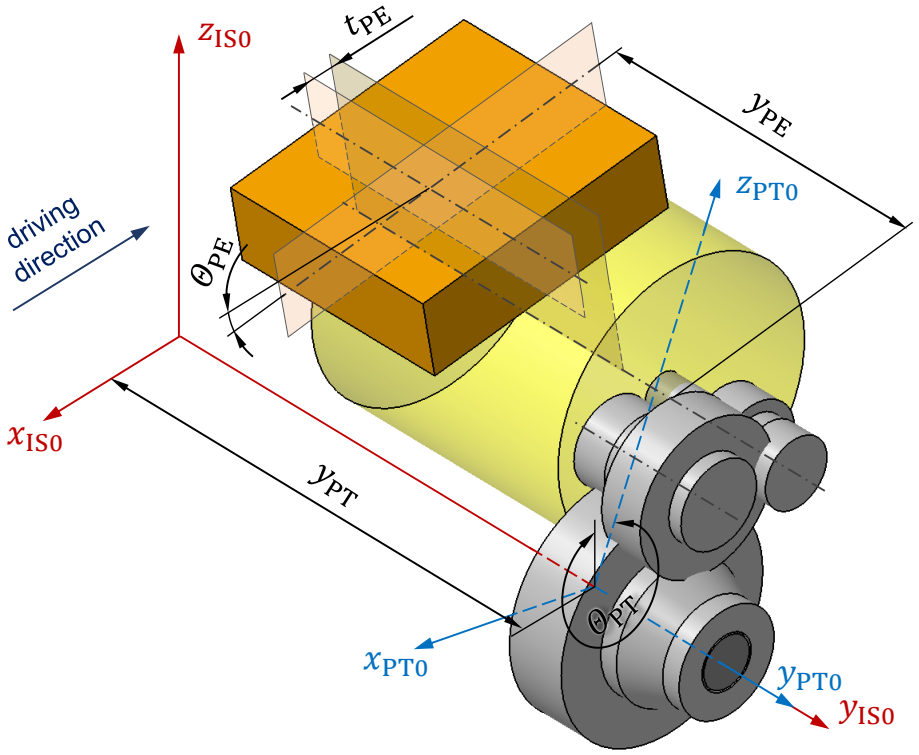

Figure 3.12: Degrees of freedom of the powertrain arrangement with respect to the installation space coordinate system

downwards in a way that results in an unacceptably low ground clearance of the vehicle or even intersections with the roadway.

To obtain a quantity based on which the package situation can be rated, a special package metric is introduced, which is defined as

$$q_{\mathrm{PM}} = \begin{cases} V_{\mathrm{iAvail}} + p_{\mathrm{Forb}} \cdot V_{\mathrm{iForb}} & \text{if } V_{\mathrm{iAvail}} > 0 \\ -c_{\mathrm{Avail}} & \text{otherwise} \end{cases}, \tag{3.63}$$

where V_{iAvail} denotes the protruding volume of the powertrain with respect to the available installation space and V_{iForb} the intersecting volume of the powertrain with the forbidden installation space. The penalty factor p_{Forb} is greater than or equal to zero and can otherwise be chosen freely. It is used to weigh intersections with the forbidden installation space stronger than protrusions with respect to the available installation space. In case there is no violation of the available space (meaning the powertrain fits inside), the negative value of the minimum clearance between powertrain and available installation space surface c_{Avail} defines the package metric. Both cases are depicted in Figure 3.13. Thus, a single scalar metric incorporating 3D shape information of the e-drive and installation space results. A minimization of the package metric directly leads

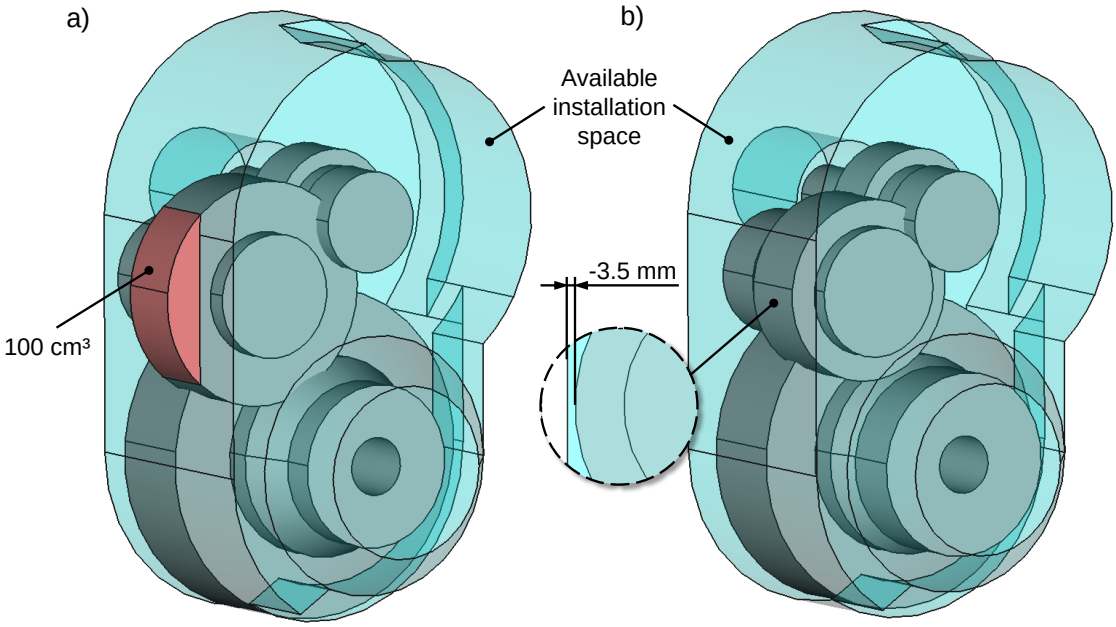

Figure 3.13: Exemplary visualization of the package metric; a) violation of available installation space, b) no violation

to favorable designs regarding package.

In general, for a certain powertrain configuration, some degrees of freedom regarding the arrangement parameters arise. Changing these parameters might result in a different package metric. Accordingly, the best arrangement needs to be found first before the value of the package metric can serve as a rating criterion. This means that the optimization problem

$$q_{\mathrm{PM\,min}} = \mathrm{minimize}\,(q_{\mathrm{PM}}) \tag{3.64}$$

needs to be solved for every single gearbox design (with a given design of electric machine and power electronics unit). Thus, a nested optimization problem is present – for every evaluation of the objective function by the actual gearbox optimization, the package metric optimization needs to be performed (in case it is an objective for the gearbox optimization).

With the described approach for assessing the package integration, there is no strict demand that a certain e-drive completely fits inside a given installation space – designs with protrusions are still valid but are rated badly. This means in case designs that would fit inside are unfeasible due to the set requirements (available installation space too small), the optimization will try to find designs with the smallest possible violation of the installation space.

3.3 Optimization Strategies

The previously presented analysis models are used to optimize the system "gearbox". The underlying optimization process is performing the actual design task as can be seen in Figure 3.2. Details regarding the gearbox optimization and the determination of the minimum package metric for a certain powertrain configuration (as discussed in section 3.2) are outlined in this section.

3.3.1 Gearbox Optimization

The requirements of the gearbox system serve as input to the design task (as illustrated in Figure 3.1) and thus describe the optimization problem. These requirements can be distinguished between

a) benchmarking requirements and

b) constrainining requirements.

Benchmarking requirements allow a comparison and rating of different gearbox designs (e.g. low costs, low losses, low mass, favorable package integration et cetera). The optimization objectives are directly derived from these. Any quantity that is determined by the analysis model can serve as objective. In general, multiple benchmarking requirements exist simultaneously and thus a multi-dimensional objective space is present. Accordingly, the application of a multi-objective optimization is required.

Constraining requirements need to be fulfilled for a valid gearbox design (e.g. service life $\geq$ 1000 h). However, once fulfilled, no further rating based on these is applied. Exemplary, a gearbox with a higher calculated service life than required does not yield a direct benefit. That way, constraining requirements are formulated as constraints for the optimization.

Concerning the design parameters, a distinction can be made between

a) variable and

b) constant parameters.

Variable design parameters are altered by the design synthesis process (see Figure 2.12) and directly represent the optimization parameters – thus in sum representing the search space. That way, the optimization process adjusts variable design parameters so that the specified benchmarking requirements are fulfilled best. An example of such a variable design parameter is the number of teeth of a gear wheel.

Constant design parameters need to be defined for the analysis model but are not altered during the optimization. This affects parameters for which a change makes no sense or is irrelevant. An example is the safety clearance between interior and housing. Especially for parameter studies, certain variable parameters might be kept constant to determine

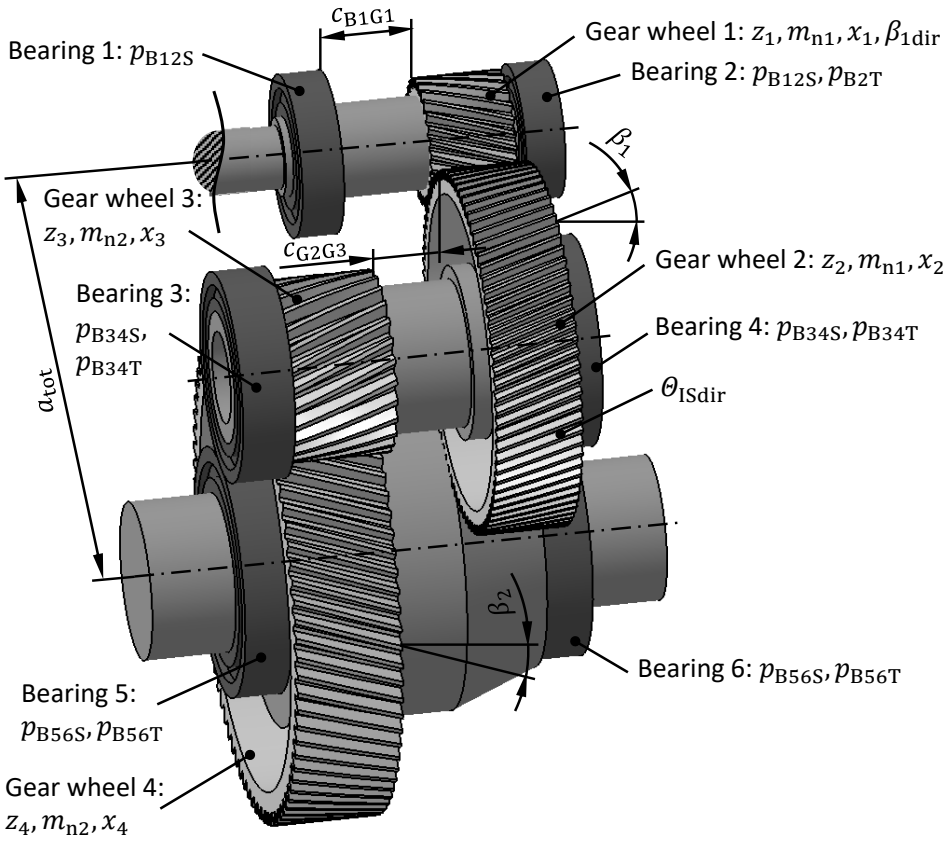

Figure 3.14: Implemented variable design parameters for a single-speed, two-stage offset gearbox with modular input shaft; variable description in Table 3.1

their influence on the system properties and thus gain additional knowledge. Deciding about which parameter is variable and which is constant is done based on the functional specification document and engineering know-how.

3.3.1.1 Objective Function

A total of 23 variable design parameters (and thus optimization parameters) are implemented for a single-speed, two-stage, offset gearbox (the most common topology – see section 2.1) with modular input shaft (see Figure 2.9) as illustrated in Figure 3.14 and listed in Table 3.1. For an integral input shaft the parameters are the same. However, the axial distance between bearing 1 and gear wheel 1 c_{B1G1} is no longer variable but a constant depending on the dimensions of the electric machine. The number of optimization parameters is thus reduced to 22.

The earlier described analysis model is used to determine the gearbox properties, which then can serve as objectives for the optimization. A simplified flow chart illustrating the

Table 3.1: Variable design parameters depicted in Figure 3.14

Parameter symbol(s)	**Description**	**Range**
z_1, z_2, z_3, z_4	Number of teeth of the single gear wheels	Problem-dependent
x_1, x_2, x_3, x_4	Profile shift coefficient of the single gear wheels	Problem-dependent
m_{n1}, m_{n2}	Normal modules of first and second gear pair	Problem-dependent
β_1, β_2	Helix angles of first and second gear pair	Problem-dependent
β_{1dir}	Helix angle direction of gear wheel 1	Right-hand, left-hand
c_{B1G1}	Axial distance between bearing 1 and gear wheel 1	Problem-dependent
c_{G2G3}	Axial distance between gear wheels 2 and 3	Problem-dependent
p_{B12S}	Selection parameter for bearings 1 and 2	$0 \ldots 1$
p_{B34S}	Selection parameter for bearings 3 and 4	$0 \ldots 1$
p_{B56S}	Selection parameter for bearings 5 and 6	$0 \ldots 1$
p_{B2T}	Type of bearing 2	Grooved ball bearing, cylindrical roller bearing
p_{B34T}	Type of bearings 3 and 4	Grooved ball bearings, tapered roller bearings
p_{B56T}	Type of bearings 5 and 6	Grooved ball bearings, tapered roller bearings
Θ_{ISdir}	Alignment direction of the intermediate shaft (see Figures 4.2 and 4.13 for a visualization of both cases)	Right-hand, left-hand
a_{tot}	Total center distance	Problem-dependent

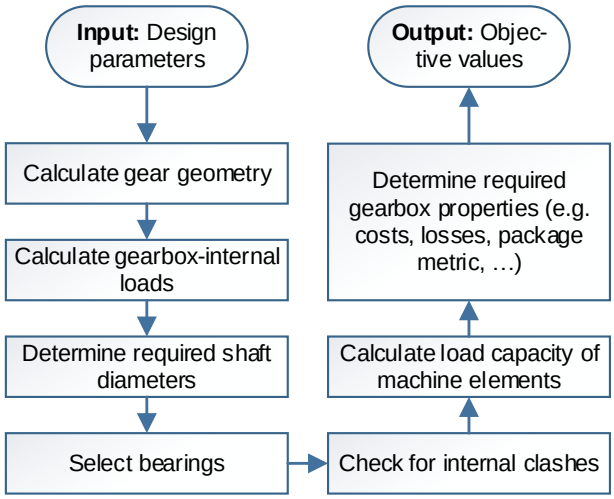

Figure 3.15: Simplified flow chart of the gearbox objective function

main steps during the evaluation of a gearbox parameter set by the objective function is shown in Figure 3.15.

Especially the bearing selection process shall be explained in more detail in the following. Provided as input are lists of certain bearings from which the optimization algorithm can choose from. These lists are filtered by geometric compatibility (e.g. remove bearings with a smaller inner diameter than the minimum required outer shaft diameter) and the bearings limiting speed. For each shaft, all bearings remaining in these filtered lists are then combined in a full factorial manner. That way, a list of bearing combinations for each shaft is obtained. The reaction forces and load capacity of every single combination is determined and bearing combinations with an insufficient load capacity are eliminated. Thus, the remaining bearing combinations are eligible for the gearbox design. The bearing selection parameters determine which combinations are actually used (0: first in the list of eligible bearing combinations, 1: last in the list of eligible bearing combinations).

At this point it should be noted, that the face widths of the gear wheels are not treated as variable design parameters but determined by requirements regarding the NVH-behavior. For favorable characteristics concerning noise, vibration and harshness an overlap ratio of $\varepsilon_\beta = 1$ or $\varepsilon_\beta = 2$ is suggested in [26]. This equality constraint can be rearranged to obtain the face width

$$b = \varepsilon_\beta \cdot \pi \cdot \frac{m_\mathrm{n}}{\sin(\beta)}. \tag{3.65}$$

3.3.1.2 Optimization Algorithm

In order to perform the actual optimization process, a corresponding algorithm is required and implemented in a numerical computing environment [19]. As the problem in general is multi-objective and a holistic design method needs to find global optima, a stochastic algorithm is chosen. In particular, differential evolution is used, which was first described by Storn and Price [40]. To allow for multi-objective optimizations, a specified number of the best designs found so far is stored in an archive. After each crossover in the evolutionary process, the entire archive is sorted according to the Pareto front rank and crowding in the objective space. That way, designs closest to the actual Pareto front, which are not surrounded by many similar designs, survive the longest. At the end of the optimization, these designs represent the found approximation of the Pareto front. More information can be found in [25] and [40].

3.3.1.3 Constraints

Constraining requirements are imposed as constraints on the optimization process. These constraints can be distinguished between

a) problem-independent and

b) problem-dependent constraints.

The former always need to be fulfilled, independent of a specific design task. Exemplary, no gearbox-internal clashes (e.g. of a gear wheel and another shaft) are allowed. The latter depend on the design problem at hand and change according to the design task. An example is that the specified service life of the gearbox needs to be fulfilled.

Furthermore, depending on the implementation details, a distinction between

a) explicit and

b) implicit constraints

can be made. Explicit constraints are implemented so that certain design parameters are adjusted in a way that the corresponding constraints are always fulfilled. Exemplary, if an impermissible undercut or too small top land thickness of a gear wheel is detected, the profile shift coefficient is adjusted so that the according limits are not exceeded. Furthermore, by inverting equality constraints, certain design parameters might be directly determinable without the need to formulate them as optimization parameters. An example is the calculation of the required face width of the gear wheels based on a given overlap ratio according to equation (3.65).

Implicit constraints have no direct effect on the design parameters. Whenever such a constraint is violated, the gearbox design is invalid and all objective values of the corresponding gearbox are set to infinite values (the worst values for a minimization problem). That way, as the optimization progresses, designs that violate implicit constraints will

Table 3.2: Problem-independent constraints

Constraint	**Type**	**Affected parameter(s)**
Gear wheels		
Impermissible undercut	Explicit	x_1, x_2, x_3, x_4
Too small top land thickness	Explicit	x_1, x_2, x_3, x_4
Gear pairs		
Too small tip clearance	Implicit	-
Too small total contact ratio	Implicit	-
Meshing in non-involute regions	Implicit	-
Gearbox		
Internal clashes	Implicit	-

vanish from the archive. They are applied whenever a corrective strategy as for explicit constraints is not applicable. Exemplary, in order to avoid a clash between a gear wheel and another shaft, the number of teeth of the corresponding gear wheel can be reduced. However, at the same time this will lower the load capacity of the gear wheel. To counteract, the module can be increased, which as a consequence enlarges the gear wheel diameter – potentially leading to a clashing situation again. In fact, this is an example for the complex interferences of single components inside a gearbox that heuristic design strategies at component level may not consider.

The implemented explicit constraints, which affect the optimization parameters described in Table 3.1, and implicit constraints are listed in Tables 3.2 and 3.3. Impermissible undercuts and too small top land thicknesses are avoided by clamping the profile shift coefficients at the corresponding lower and upper limit whenever they are exceeded. Upper and lower limits for the face width to diameter ratios

$$\Psi_{\mathrm{d}} = \frac{b}{d} \tag{3.66}$$

are implemented to prevent designs with unfavorable stiffness characteristics (e.g. large diameter and very small face width). By adjusting the helix angles the face width is adapted so that the limits are not exceeded (see equation (3.65) for the relation).

The bearing selection process has already been described in section 3.3.1.1. Depending on geometrical constraints, maximum shaft rotational speeds and requirements concerning the load capacity, lists of eligible bearing combinations are generated for each shaft. Accordingly, these lists are influenced by the set requirements. The selection parameters p_{B12S}, p_{B34S}, p_{B56S} thus might map to other bearing combinations when the requirements

Table 3.3: Problem-dependent constraints

Constraint	**Type**	**Affected parameter(s)**
Gear wheels		
Limits to face width to diameter ratio Ψ_d	Explicit	β_1, β_2
Root diameter smaller than required shaft diameter	Implicit	-
Gear pairs		
Sufficient load capacity	Implicit	-
Bearings		
Geometric compatibility	Explicit	p_B12S, p_B34S, p_B56S
Sufficient limiting speed	Explicit	p_B12S, p_B34S, p_B56S
Sufficient load capacity	Explicit	p_B12S, p_B34S, p_B56S
Gearbox		
Total transmission ratio	Explicit	z_1, z_2, z_3, z_4
Total center distance achievable	Implicit	-
Limits to main dimensions	Implicit	-

are changed.

In order to obtain a design with a proper transmission ratio (target transmission ratio and a certain tolerance), all eligible combinations of teeth numbers are identified first. The optimization algorithm is then selecting from this list of teeth number combinations. Furthermore, depending on the single center distances of the two gear pairs (which result from the gear-related design parameters), certain required total center distances might not be achievable (too large or too small). This situation is handled by an implicit constraint.

3.3.2 Package Metric Optimization

As already described in section 3.2, an optimization of the package metric for a certain powertrain to find the best arrangement has to be performed. Only once this minimum package metric $q_\mathrm{PM\,min}$ is found, it can be used as rating criterion describing the package situation.

Figure 3.16 shows an example of how the package metric changes with respect to the arrangement angle of the power electronics unit Θ_PE for various values of the penalty factor p_Forb. It can be seen that potentially multiple local optima exist in the objective

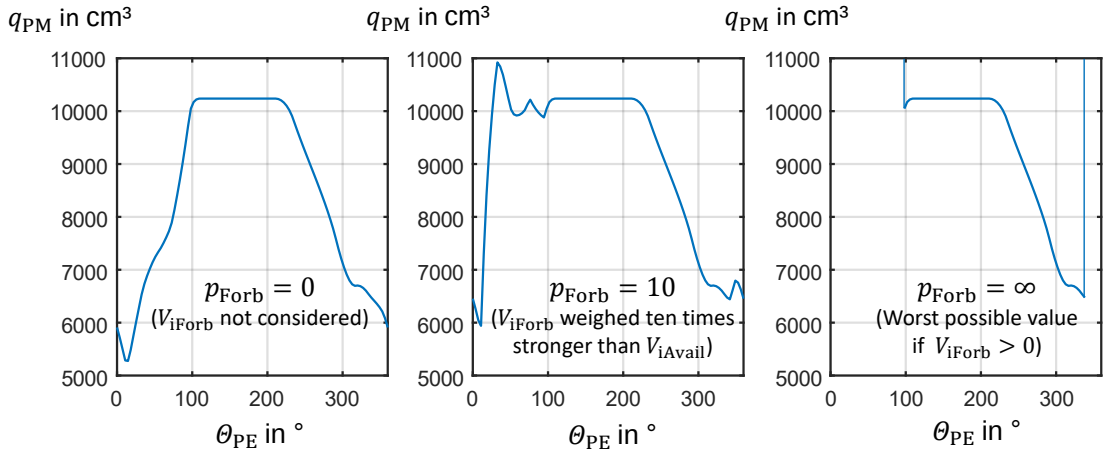

Figure 3.16: Exemplary relation between package metric q_{PM} and arrangement angle of the power electronics unit Θ_{PE} for various values of the penalty factor p_{Forb}

function, implying that a global search algorithm is required. However, the computation of the package metric is time consuming and has to be performed for every single gearbox design suggested by the stochastic gearbox optimization. Due to considerations regarding the computation time and effort, a global optimization algorithm is unsuited to find $q_{PM\,min}$. Instead, a hybrid algorithm consisting of a global and subsequent local optimization is employed. During the pre-search phase, a deterministic global algorithm (dividing rectangle [21]) tries to find a good starting point for the local algorithm (Nelder-Mead [28]), which determines the best value of the package metric. That way, a global convergence behavior is obtained.

Concerning constraints, for all arrangement parameters shown in Figure 3.12 upper and lower bounds are defined, which are chosen depending on the shape of the installation space. Furthermore, the power electronics unit might intersect the gearbox if an invalid axial offset y_{PE} is used. This is currently addressed by properly setting the bounds for y_{PE} and otherwise not further investigated.

4 Results & Discussion

In the following section, the presented design method is applied for two case studies. The results are discussed and the found solution set is compared to conventionally engineered reference solutions to verify the method.

The first case study involves a completely separated gearbox design task. All requirements, including the installation space, are explicitly given for the gearbox. The second case study involves a design task for the entire system "e-drive". This also means the given installation space is intended to accommodate the power electronics unit, electric machine and gearbox. The design of the power electronics unit and the design of the electric machine are given as inputs to the gearbox optimization and are not altered.

4.1 Case Study A

For the first case study, a completely separated gearbox design task is presented. This means all requirements, including the installation space, are explicitly given for the gearbox. The main requirements are listed in Table 4.1, the available installation space is shown in Figure 4.1. No forbidden installation space is considered. As the gearbox design is separated from the electric machine, a modular design of the input shaft is chosen. Moreover, based on the shape of the installation space, topology type 1 (see Figure 2.10) is used. All parameters listed in Table 3.1, except for the total center distance a_{tot} (constant), are subject to optimization.

This case study has already been presented in a previous publication [16]. However, as the analysis model and the synthesizing strategy have been refined since, the results differ. Furthermore, an oil of ISO viscosity class VG 220 has been applied in [16].

The optimization is configured to minimize the objectives

a) costs,

b) losses,

c) package metric and

d) the number of unique bearings.

The losses are determined by application of a longitudinal vehicle dynamics model, which is used to simulate the WLTP class 3 cycle. Braking of the vehicle is done entirely by recuperating. The degree of losses is then obtained according to equation (3.51).

Table 4.1: Main requirements for case study A

Total transmission ratio	$9.32 \pm 1\,\%$
Total center distance	165 mm
Nominal input torque	366 Nm
Maximum input speed	15 000 rpm
Required service life	944 h
Material of shaft & gears	20MnCr5
Oil	ISO VG 46

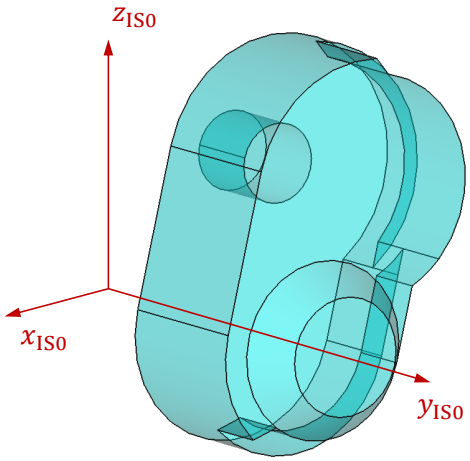

Figure 4.1: Visualization of the available installation space for case study A

Furthermore, a degressive cost model for the bearings according to equation (3.62) is applied. This means both an explicit and an implicit common-part approach as described in section 3.1.5 are employed. However, this is only done for a better visualization of the trade-off between the number of unique bearings and the actual system costs (later explained in greater detail).

The optimization algorithm is configured according to Table 4.2. Only the axial position of the powertrain y_{PT} is subject to the package metric optimization. The tilt angle Θ_{PT} is a known constant defined by the given location of the input shaft axis. The optimization is terminated after 1200 generations, which corresponds to about 20 hours of computation time on a standard workstation computer equipped with four physical CPU cores. With this number of generations repeatable results were achieved.

The final set of designs contains 534 Pareto-optimal solutions. As a four-dimensional objective space is present that can not be directly visualized, single two-dimensional projections are used to visualize the results in the following. Furthermore, a fully engineered

Table 4.2: Main configuration of the optimization algorithm for case study A (refer to [40])

Population size	200
Archive size	2000
Mutation strategy	One random difference and a difference to current best
Mutation factors	Random difference: 0.6 Difference to current best: 0.6
Crossover strategy	Independent binomial experiments
Crossover constant	0.5
Optimization parameters for $q_{\mathrm{PM\,min}}$	y_{PT}

reference solution for this case study is known (depicted in Figure **??** and evaluated by the presented analysis models. That way, this reference solution can be compared to the solution set found by the optimization algorithm and used to verify the method. However, it should be noted that the reference solution is equipped with a park lock at the input shaft, which has not been included in the present optimization. This has to be considered when comparing the values.

4.1.1 Extreme Designs

Some properties of the found extreme designs for the objectives costs, losses and package metric as well as the reference solution are given in Table 4.3. Figure 4.2 shows a CAD-visualization of the reference solution and the found extreme designs. The violating volume of the available installation space is depicted in red color.

It can be seen that compared to the reference solution a cost reduction of up to 25 %, a reduction of the degree of losses of up to 15.7 % and a reduction of the package metric of up to 86.6 % is feasible. However, non of these improvements are achievable simultaneously. The cost-optimal solution also shows a better package-integration but the losses are higher. The efficiency-optimal solution shows higher costs and especially a drastically higher package metric than the reference design. For the package-optimal solution the costs are lower than for the reference design but the losses again are higher. This means a certain conflict between the single objectives is present justifying the multi-objective optimization approach. Furthermore, the package metric of the package-optimal solution has a value greater than zero. This means for the defined problem no solution exists that completely fits inside the available installation space. As can be seen in Figure 4.2, a certain violation at the intermediate shaft has to be accepted.

Table 4.3: Reference and extreme designs for case study A

	Reference	**Cost-optimal**	**Efficiency-optimal**	**Package-optimal**
Relative costs	100 %	75 %	116 %	88 %
Degree of losses	2.10 %	2.29 %	1.77 %	2.21 %
Package metric in cm^3	127	83	2130	17
z_1, z_2, z_3, z_4	27, 83, 27, 82	30, 74, 26, 99	33, 109, 32, 91	26, 63, 25, 95
m_{n1}, m_{n2} in mm	1.57, 2.20	1.61, 2.03	1.47, 2.34	1.70, 2.07
Bearing 1	6206	6307	6305	6307
Bearing 2	NU205-E	6307	NU305-E	NU206-E
Bearing 3	32010	30207	6407	30207
Bearing 4	32010	30207	6308	30207
Bearing 5	6012	6311	6311	6311
Bearing 6	6011	6210	6211	6210

The very high package metric of the efficiency-optimal solution is due to the large gear wheels required to minimize the gearbox-internal loads – large gear wheel diameters result in large lever arms and thus lower forces. This means the load-dependent losses at the gear wheels and bearings are reduced but at the same time the velocity-dependent losses are increased due to higher circumferential velocities. Apparently, for this case study the former are dominant and the lowest possible losses are achieved by large gear wheel diameters compared to the available installation space.

4.1.2 Efficiency Trade-Offs

To visualize the trade-offs in the solution set embodied by the Pareto front, a first comparison between costs and losses as well as package-integration and losses is made. The projection of the Pareto front in the dimensions "costs" and "losses" is shown in Figure 4.3, the reference solution is marked with "Ref". A conflict between these two objectives can be seen – solutions with low costs show high losses and vice versa. Another interesting aspect depicted in Figure 4.3 is the influence of the bearing types. A total of four different bearing type combinations lead to optimal solutions for this case study,

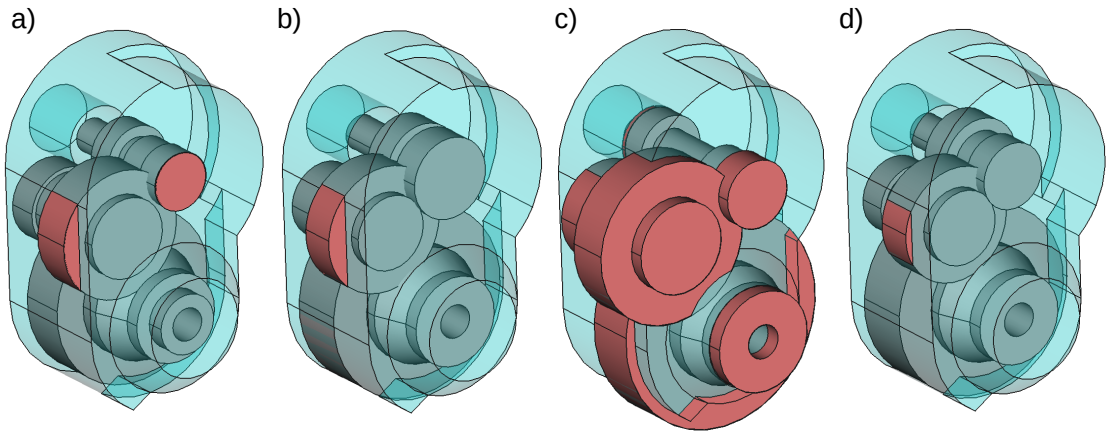

Figure 4.2: CAD-visualization of the reference solution and found extreme designs for case study A; a) reference design, b) cost-optimal solution, c) efficiency-optimal solution, d) package-optimal solution

which are (see Figure 3.14 for bearing numbering)

a) GBB, GBB, GBB: all bearings are grooved ball bearings;

b) GBB, TRB, GBB: grooved ball bearings on the input and output shaft, tapered roller bearings on the intermediate shaft;

c) CRB, GBB, GBB: bearing 2 is a cylindrical roller bearing, all other are grooved ball bearings;

d) CRB, TRB, GBB: bearings 1, 5 and 6 are grooved ball bearings, bearing 2 is a cylindrical roller bearing and bearings 3 and 4 are tapered roller bearings.

The reference solution belongs to cluster ”CRB, TRB, GBB” and shows comparable costs and losses with all other solutions in this group. However, only investigating these two objectives, all other clusters dominate ”CRB, TRB, GBB” and are thus more favorable if low losses and costs are highly important in the context of the design problem.

Solutions with a cylindrical roller bearing for bearing 2 and otherwise grooved ball bearings (CRB, GBB, GBB) show the lowest losses but are rather expensive. Solutions with only grooved ball bearings (GBB, GBB, GBB) represent a balanced trade-off between both objectives and solutions with tapered roller bearings at the intermediate shaft and otherwise grooved ball bearings (GBB, TRB, GBB) show the lowest costs but also high losses. General engineering knowledge implies that grooved ball bearings are favorable for low losses [3]. Frankly, this is not entirely true in this case study. Bearing 2 has to support high radial loads, which requires seriously larger grooved ball bearings compared to cylindrical roller bearings due to their lower load capacity. This also means that frictional forces have a larger lever arm and thus induce a higher frictional torque than cylindrical roller bearings.

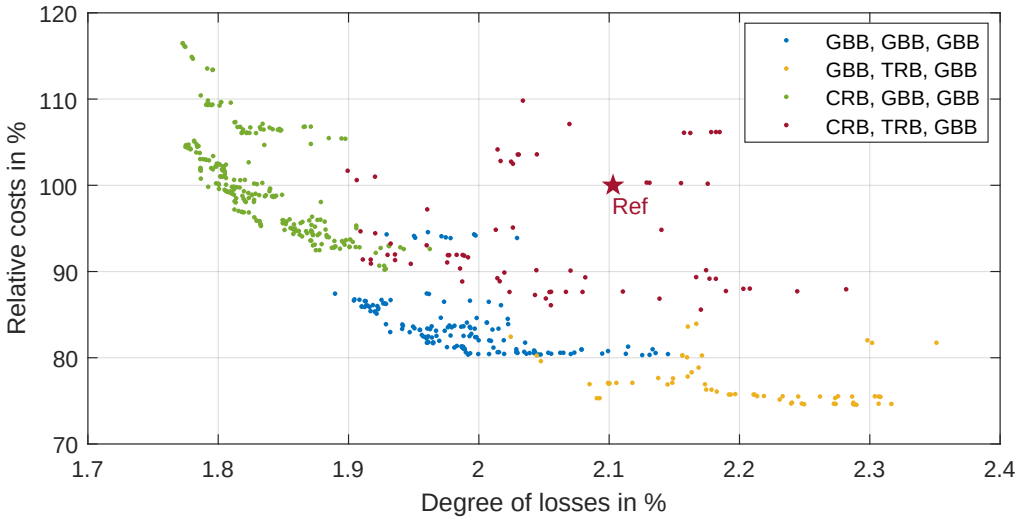

Figure 4.3: Projection of the Pareto front in the dimensions "costs" and "losses" for case study A

Another conflict between the objectives "package metric" and "losses" is illustrated in Figure 4.4, which shows a projection of the Pareto front in these two dimensions. Contrary to the projection in Figure 4.3, the cluster "CRB, TRB, GBB" now particularly shows its strength when a favorable package-integration is of high importance as the lowest package metrics are achieved. Furthermore, a well balanced trade-off between package metric and losses is embodied by "CRB, TRB, GBB". The only other non-dominated cluster is "CRB, GBB, GBB", which is due to its low degree of losses but otherwise rather bad package rating.

4.1.3 Common-Part Aspects

As explained earlier, both an explicit and implicit common-part approach (see section 3.1.5) are chosen for the optimization. Thus, the number of unique bearings is explicitly minimized and additionally a degressive cost model is applied. That way, the actual influence of the number of unique bearings on the costs and the other objectives can be better visualized – designs with the lowest possible number of unique bearings are present in the solution set regardless of their actual optimality regarding the other objectives.

As can be seen in Figure 4.5, a minimum of three unique bearings is eligible for this design problem. Depicted is the conflict and thus trade-off between the objectives "package metric" and "number of unique bearings". It can be seen that solutions with six (the highest possible number) and five unique bearings show the best package metrics. In fact, changing from six to five different bearings is a design decision that almost has no influence on the package integration in the extreme case. However, changing to

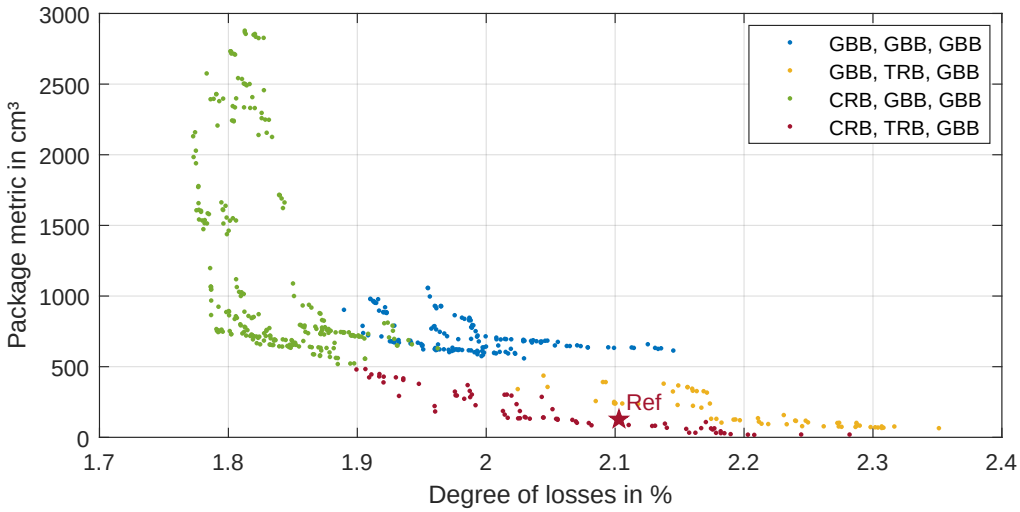

Figure 4.4: Projection of the Pareto front in the dimensions "package metric" and "losses" for case study A

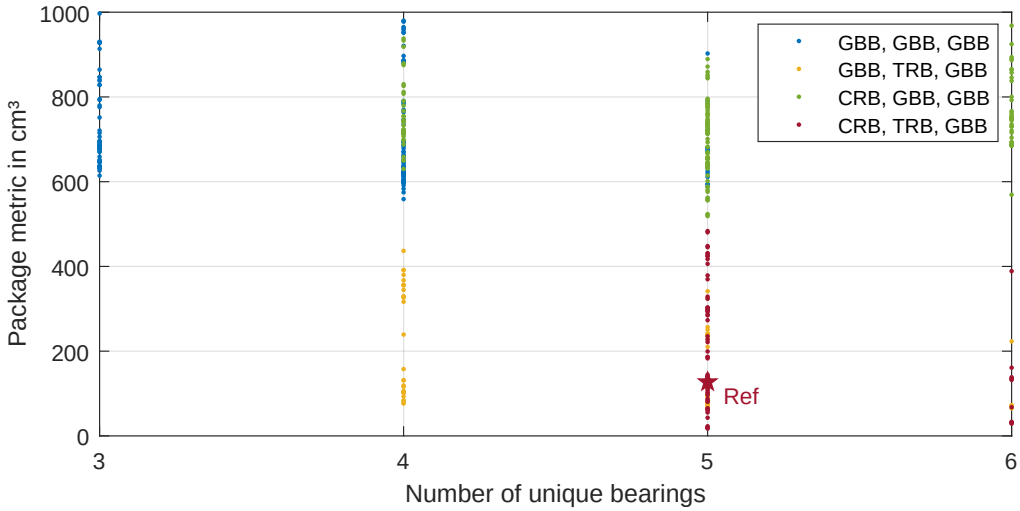

Figure 4.5: Projection of the Pareto front in the dimensions "package metric" and "number of unique bearings" for case study A (only solutions with a package metric smaller than 1000 cm^3 are shown)

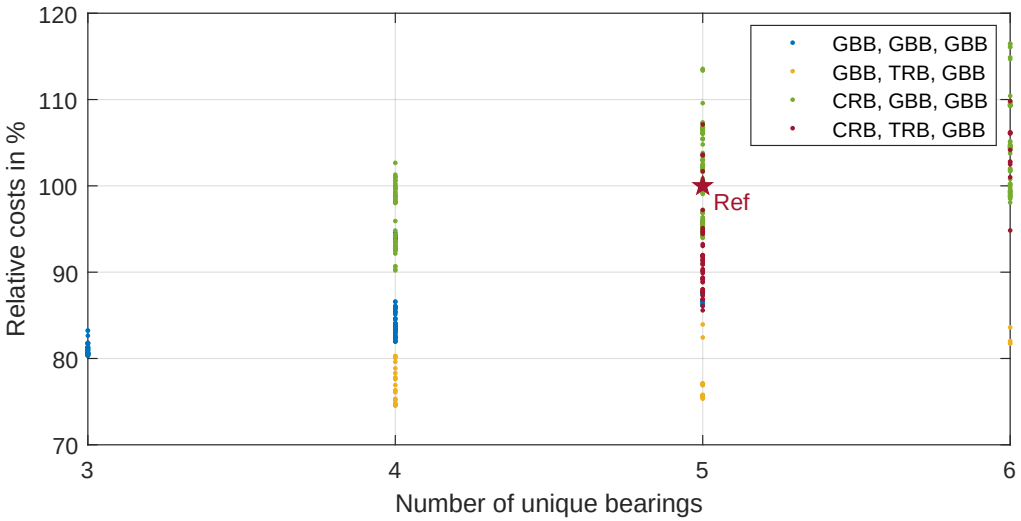

Figure 4.6: Projection of the Pareto front in the dimensions ”costs” and ”number of unique bearings” for case study A

four unique bearings has a small impact and changing to three unique bearings has a large impact on the package integration. This outlines the consequences of enforcing a common-part approach by explicitly minimizing the number of unique bearings – other objectives, in this case the package metric, might take unacceptable values.

To visualize the actual relation between the number of unique bearings and the costs in the system context, the projection in the dimensions ”costs” and ”number of unique bearings” is depicted in Figure 4.6. It can be seen that the global cost optimum is achieved by only four unique bearings. Further reducing this number actually increases the costs again and potentially has unfavorable consequences concerning the other objectives (e.g. the package metric as shown in Figure 4.5). In fact, some solutions with five unique bearings are even cheaper than designs with three unique bearings. It can be concluded that no direct correlation between a simple explicit common-part approach (minimization of the number of unique bearings) and the actual cost benefit is present. Although an explicit approach does not require a sophisticated cost model, the resulting solution set might lead to wrong conclusions for the system costs and has to be handled with care.

4.1.4 Influence of the Applied Material

An investigation of the obtained solution set revealed that tooth root bending fatigue is critical for most designs. Compared to the original material 20MnCr5, the more expensive high-strength material 18CrNiMo7-6 shows a higher resistance against tooth root bending fatigue [39]. The question arises, if the package integration can be improved by application of this high-strength material and how big the cost impact is. To find

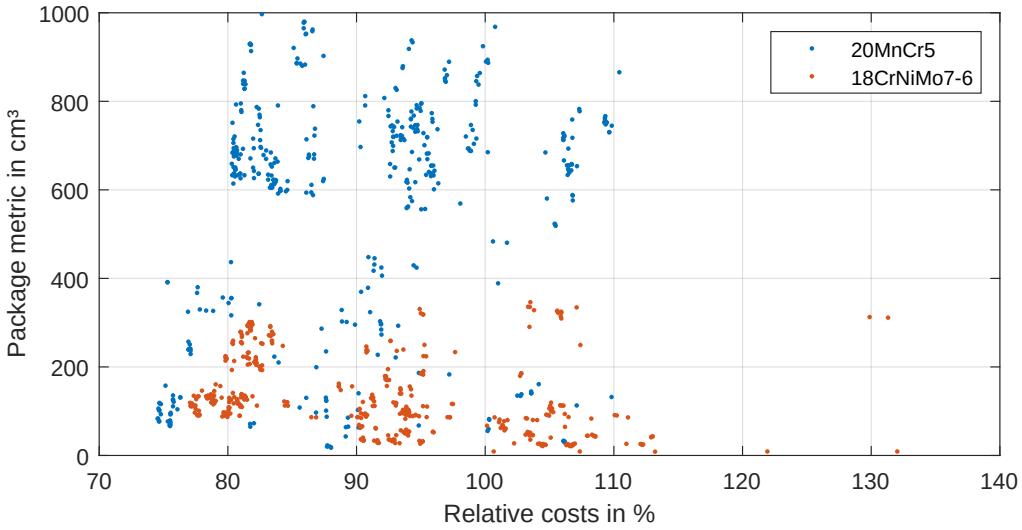

Figure 4.7: Projection of the Pareto front in the dimensions "package metric" and "costs" for case study A and different applied materials (only solutions with a package metric smaller than 1000 cm^3 are shown)

an answer, the same optimization is performed with 18CrNiMo7-6 as material for the shafts and gears.

A comparison of both solution sets in the dimensions "package metric" and "costs" is shown in Figure 4.7. The change of material indeed has the expected effect of lowering the package metric – most solutions have a package metric smaller than 200 cm^3. The package-optimal solution now shows a package metric of 8.5 cm^3 (17 cm^3 for 20MnCr5) but still does not completely fit inside the available installation space (still intersections at the intermediate shaft). Furthermore, in the investigated two dimensions the high-strength material is only beneficial in the region of the lowest package metrics. Elsewhere, 20MnCr5 is optimal due to the lower costs.

However, the situation is different when the Pareto front is projected in the dimensions "package metric" and "losses" as visualized in Figure 4.8. Especially in the region of low losses, solutions based on 18CrNiMo7-6 show a significantly lower package metric.

4.1.5 Influence of the Oil Viscosity

In general, higher oil viscosities are beneficial for the load capacity of the bearings and gears inside a gearbox but at the same time induce high power losses. Due to efficiency considerations, as already mentioned, oils with very low viscosity are applied in e-drives. However, as this reduces the load capacity, a potential conflict between efficiency, package integration and costs arises based on the oil selection.

In order to determine the influence of the oil viscosity, the same optimization is performed

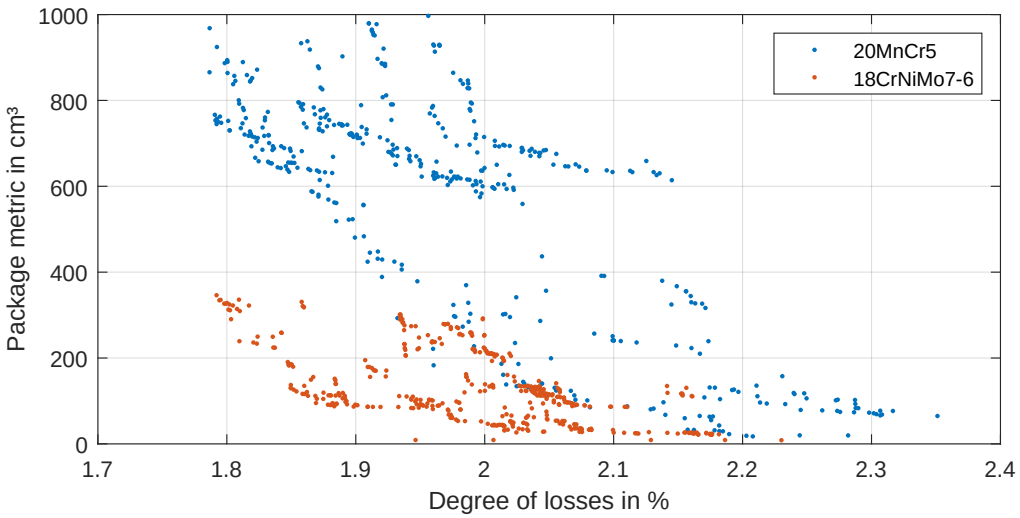

Figure 4.8: Projection of the Pareto front in the dimensions "package metric" and "losses" for case study A and different applied materials (only solutions with a package metric smaller than 1000 cm^3 are shown)

with a more viscous oil of ISO viscosity class VG 220. Especially the trade-off between package metric and losses, depicted in Figure 4.9, is of interest but also the influence of the oil selection on the system costs, shown in Figure 4.10.

First of all, it can be seen that the losses increase drastically by an absolute value of approximately 1 % (which corresponds to a relative loss increase of around 50 %) for the higher oil viscosity. However, it should be noted that low oil viscosities are not in general beneficial for the degree of efficiency. In the operating domain of high torques and low velocities, higher viscosities result in a better lubrication film quality especially at the gears and thus smaller losses. Only in the domain of low torques and high velocities, lower oil viscosities are beneficial. The operating points within the WLTP class 3 cycle are mostly in the latter domain for this case study, explaining the high impact on the degree of losses. Figure 4.11 shows the calculated efficiency map for the reference gearbox (ISO VG 46) and visualizes this situation.

Besides the decreased efficiency of the gearbox, the package integration has been drastically improved. The anticipated increased load capacity of the bearings and gears leads to multiple solutions with a negative package metric – meaning they fit inside the available installation space. The package-optimal solution for ISO VG 220 shows a package metric of -5.2 mm. The more compact designs possible for a higher oil viscosity have a direct impact on the system costs as shown in Figure 4.10. The cost-optimal solution shows a cost reduction of 37 % compared to the reference design, which uses an oil of ISO viscosity class VG 46.

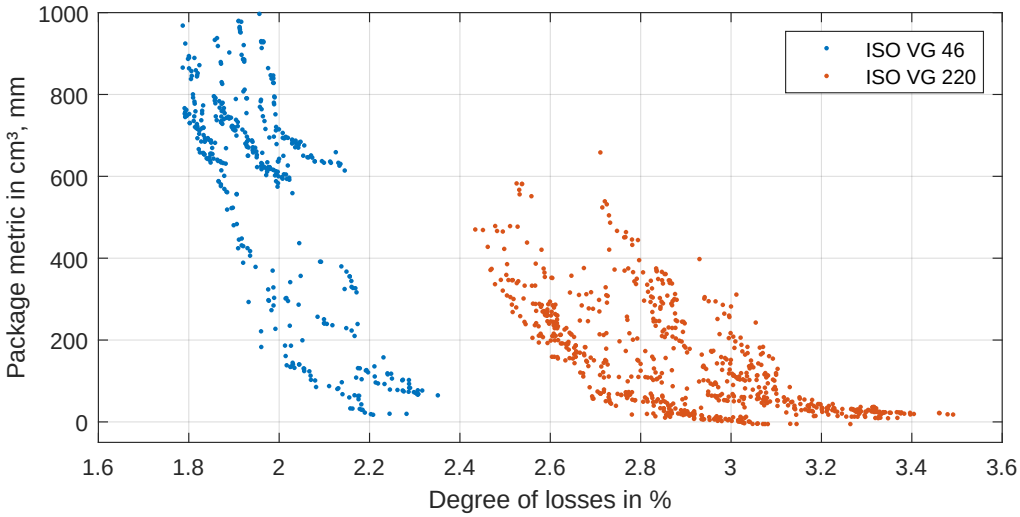

Figure 4.9: Projection of the Pareto front in the dimensions ”package metric” and ”losses” for case study A and different applied oils (only solutions with a package metric smaller than 1000 cm^3 are shown)

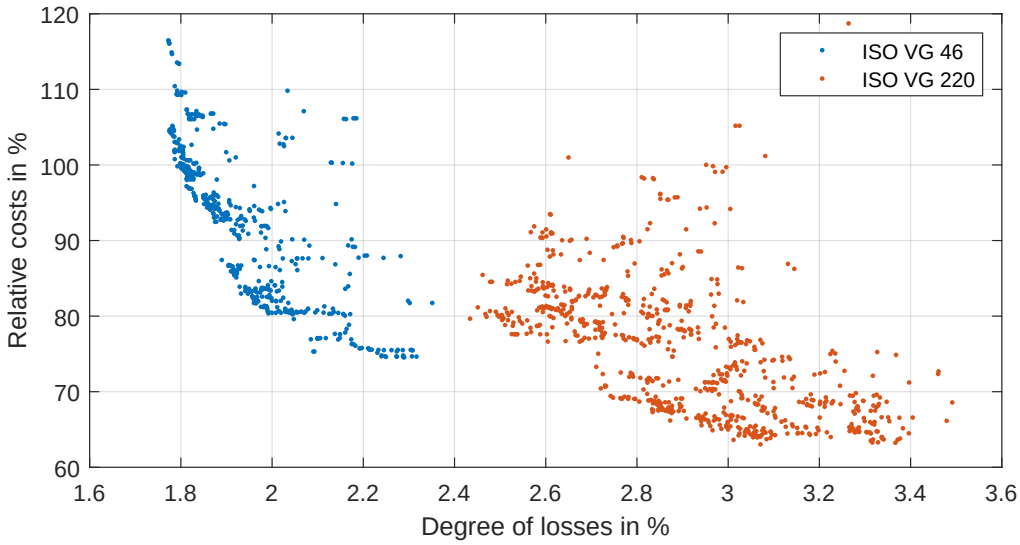

Figure 4.10: Projection of the Pareto front in the dimensions ”costs” and ”losses” for case study A and different applied oils

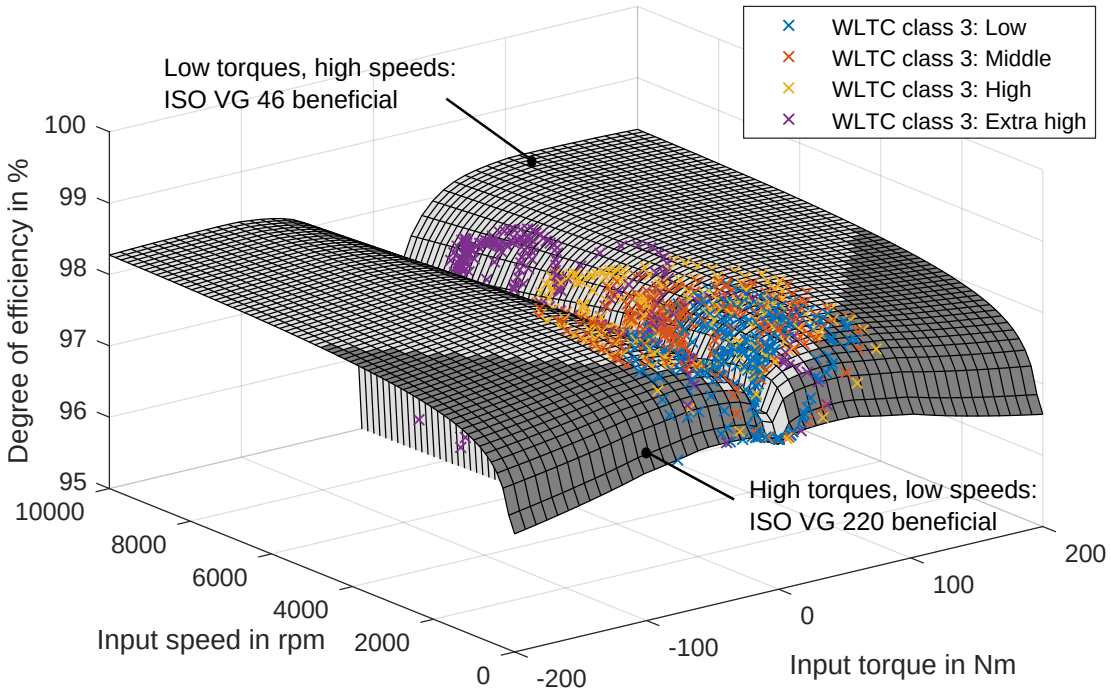

Figure 4.11: Calculated efficiency map for the reference gearbox of case study A

4.2 Case Study B

The second case study presents a design problem for the entire system "e-drive". This means the installation space is now given for the full drive unit, as illustrated in Figure 4.12. In addition to the available installation space, a forbidden space is now defined that should be avoided for a sufficient ground clearance of the vehicle. The electric machine and power electronics unit are separately designed from the gearbox, exemplary as explained in [15]. Their configurations serve as input to the gearbox design method and their geometric shapes are also depicted in Figure 4.12. The main requirements are listed in Table 4.4. Contrary to case study A, an integral design of the gearbox input shaft is now chosen. Based on the shape of the installation space, topology types 3 and 4 (see Figure 2.10) are of high interest. Optimizations for both types have been performed. However, topology type 4 in general proved to be more favorable regarding the package integration, which is why only the results of this type are presented in the following. All parameters listed in Table 3.1 except for the axial distance between bearing 1 and gear wheel 1 c_{B1G1} (as described an integral design of the input shaft does not posses this parameter) and the alignment direction of the intermediate shaft Θ_{ISdir} (manually derived from the shape of the installation space) are subject to optimization.

Table 4.4: Main requirements for case study B

Total transmission ratio	$11.09 \pm 1\,\%$
Total center distance	120 mm - 157 mm
Nominal input torque	158 Nm
Maximum input speed	15 000 rpm
Required service life	1287 h
Material of shaft & gears	20MnCr5
Oil	ISO VG 46
Electric machine	Predefined design
Power electronics unit	Predefined design

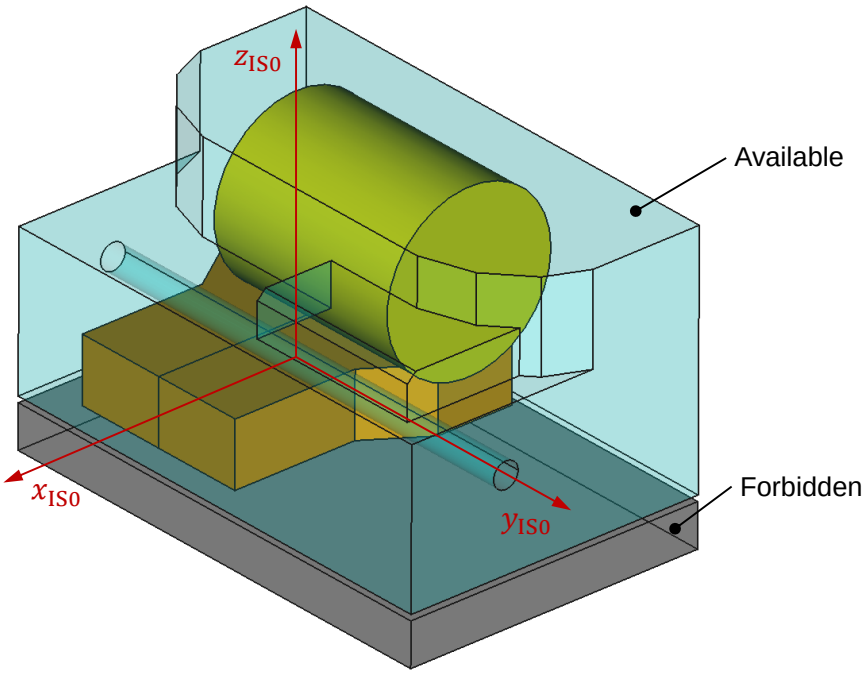

Figure 4.12: Visualization of the available and forbidden installation space for case study B

Table 4.5: Main configuration of the optimization algorithm for case study B (refer to [40])

Population size	200
Archive size	2000
Mutation strategy	One random difference and a difference to current best
Mutation factors	Random difference: 0.6 Difference to current best: 0.6
Crossover strategy	Independent binomial experiments
Crossover constant	0.5
Optimization parameters for $q_{\mathrm{PM\,min}}$	y_{PT}, Θ_{PT}
Penalty factor p_{Forb} for $q_{\mathrm{PM\,min}}$	10

The optimization is configured to minimize the objectives

a) costs,

b) losses and

c) the package metric.

The losses are determined in the same manner as for case study A (WLTC). Furthermore, a degressive cost model for the bearings according to equation (3.62) is applied. The optimization algorithm is configured similarly to case study A (Table 4.5). However, as more degrees of freedom concerning the powertrain arrangement are now present, the axial position y_{PT} and the powertrain tilt angle Θ_{PT} are altered during the package metric optimization. The position of the power electronics unit is kept constant as shown in Figure 4.12. Based on the shape of the installation space and power electronics unit, hardly any other positions are reasonable.

The optimization is terminated after 600 generations as repeatable results where achieved after this number of generations on multiple runs. The final set of designs contains 369 Pareto-optimal solutions, which again are compared to a fully engineered reference design evaluated by the presented analysis models. It should be noted that the reference design uses topology type 3 instead of type 4.

4.2.1 Extreme Designs

Again, the found extreme designs regarding the set objectives are investigated first. Table 4.6 lists some properties of the extremes and the reference solution. Figure 4.13

Table 4.6: Reference and extreme designs for case study B

	Reference	**Cost-optimal**	**Efficiency-optimal**	**Package-optimal**
Relative costs	100 %	73 %	93 %	115 %
Degree of losses	2.11 %	1.95 %	1.72 %	2.05 %
Package metric	-2.3 mm	51.97 cm^3	5.53 cm^3	-5 mm
z_1, z_2, z_3, z_4	27, 85, 23, 81	33, 91, 33, 134	33, 106, 33, 115	30, 96, 30, 105
m_{n1}, m_{n2} in mm	1.25, 1.87	1.26, 1.51	1.21, 1.64	1.18, 1.66
Bearing 1	6008	6304	6304	6304
Bearing 2	NU205-E	6306	NU304-E	NU206-E
Bearing 3	30206	6306	30206	32008
Bearing 4	30206	6308	30206	32008
Bearing 5	LM503349-A-LM503310	6010	6011	6011
Bearing 6	LM503349-A-LM503310	6212	6212	6213

shows a corresponding CAD-visualization.

It can be seen that compared to the reference solution a cost reduction of up to 27 % and a reduction of the degree of losses of up to 18.5 % are feasible. The reference design and the package-optimal solution both show a negative package metric, which means both solutions fit inside the given installation space. An investigation of the corresponding 3D-CAD models revealed that the electric machine can be more critical concerning the package integration than the gearbox. This is why the reference design shows a worse package rating than the package-optimal solution even whilst a more compact gearbox design is present for the reference design – the larger center distance of the reference design moves the electric machine closer to the boundary of the available installation space.

In this case study, the cost-optimal solution shows a much higher package metric than the efficiency-optimal one. This is primarily due to the fact that the smaller load compared to case study A allows the application of also smaller and thus cheaper grooved ball bearings. However, this does not simultaneously mean such a design is most favorable for the gearbox efficiency. It can be seen in Table 4.6 that the efficiency-optimal gearbox makes use of a cylindrical and two tapered roller bearings. As already described in section 4.2.1, an important influence on the losses is the lever arm of the frictional forces

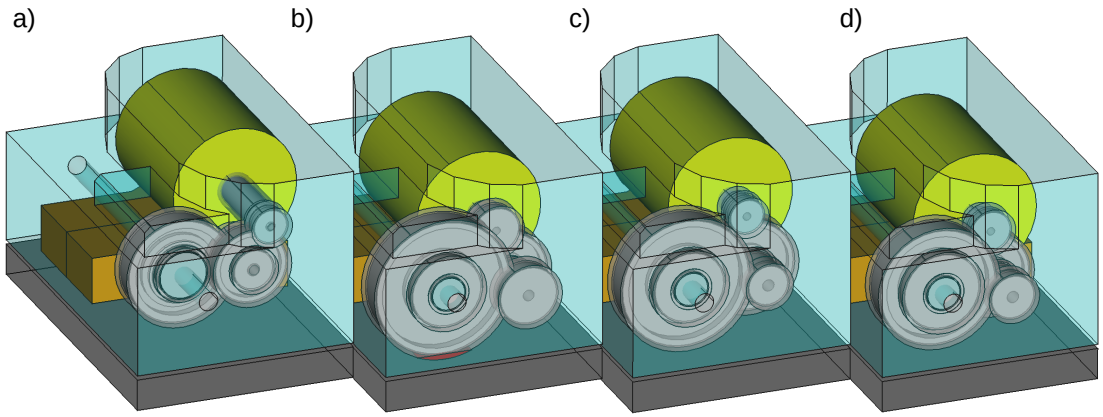

Figure 4.13: CAD-visualization of the reference solution and found extreme designs for case study B; a) reference design, b) cost-optimal solution, c) efficiency-optimal solution, d) package-optimal solution

and thus the bearing diameter. However, designs with grooved ball bearings at the intermediate shaft can compete (partially at the cost of a very bad package rating), as will be shown in the next section.

4.2.2 Efficiency Trade-Offs

Projections of the Pareto front in the dimensions ”degree of losses” and ”costs” as well as ”degree of losses” and ”package metric” are chosen again to visualize the solution set. As can be seen in Figure 4.14, the same types of bearing combinations as for case study A lead to optimal solutions. However, the reference design employs a grooved ball bearing for bearing 1, a cylindrical roller bearing for bearing 2 and tapered roller bearings for all other locations (CRB, TRB, TRB). This combination is absent in the solution set but, as outlined before, the reference design makes use of a different topology for which this combination might be favorable.

The clusters ”CRB, TRB, GBB” and ”CRB, GBB, GBB” represent designs with the lowest degree of losses but also high costs. Contrary, clusters ”GBB, GBB, GBB” and ”GBB, TRB, GBB” show low costs and higher losses. When compared to the solution set of case study A, a gap in-between both regions in Figure 4.14 is observable, meaning a balanced trade-off between costs and losses appears to be unfeasible for the present design problem.

Furthermore, when investigating the package metrics in the solution set, six designs with a very high metric are noticeable as depicted in Figure 4.15. These designs intersect the forbidden installation space and are thus rated badly. However, they still represent a very good trade-off between costs and losses – all of them are non-dominated in these two dimensions. Whether or not the corresponding designs are still eligible in the light of their

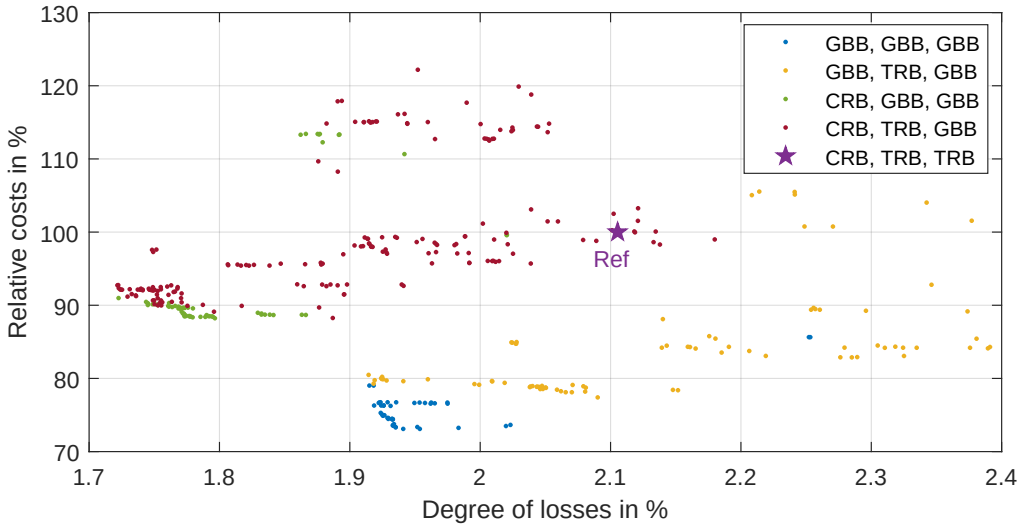

Figure 4.14: Projection of the Pareto front in the dimensions "costs" and "losses" for case study B

favorable costs-losses-trade-off is case-dependent and needs to be decided considering all aspects of the design problem. Nevertheless, more than 80 % of the solutions show a package metric smaller than 30 cm^3 and 54 % fully fit inside the available installation space. As can be seen in Figure 4.16, especially the clusters "CRB, TRB, GBB" and "GBB, TRB, GBB" show the lowest package metrics.

It can be concluded, that bearing combination types "CRB, TRB, GBB" and "GBB, TRB, GBB" show particular strengths for this design problem. The former allow for low degrees of losses at higher costs, the latter for low costs at higher degrees of losses, while both show a favorable package integration.

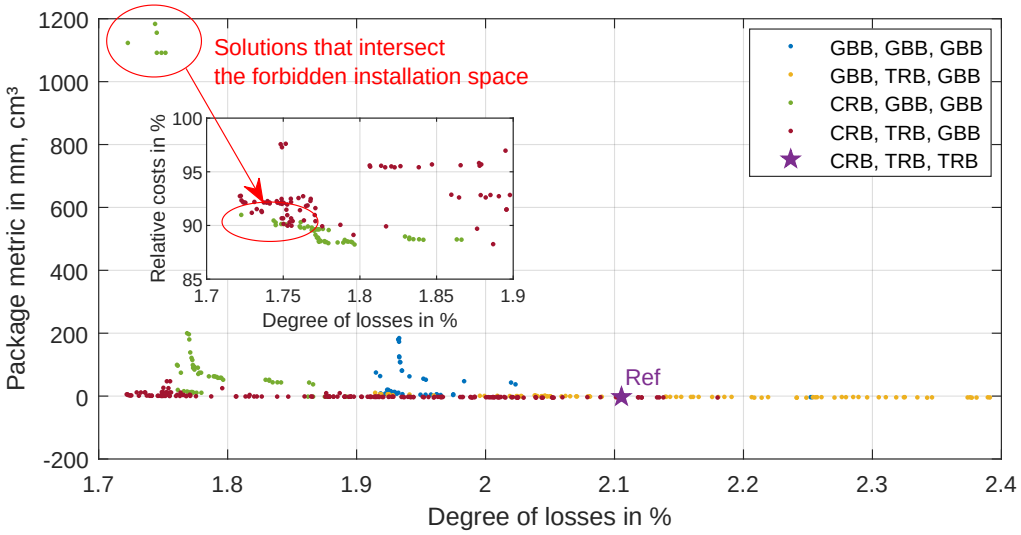

Figure 4.15: Projection of the Pareto front in the dimensions "package metric" and "losses" for case study B

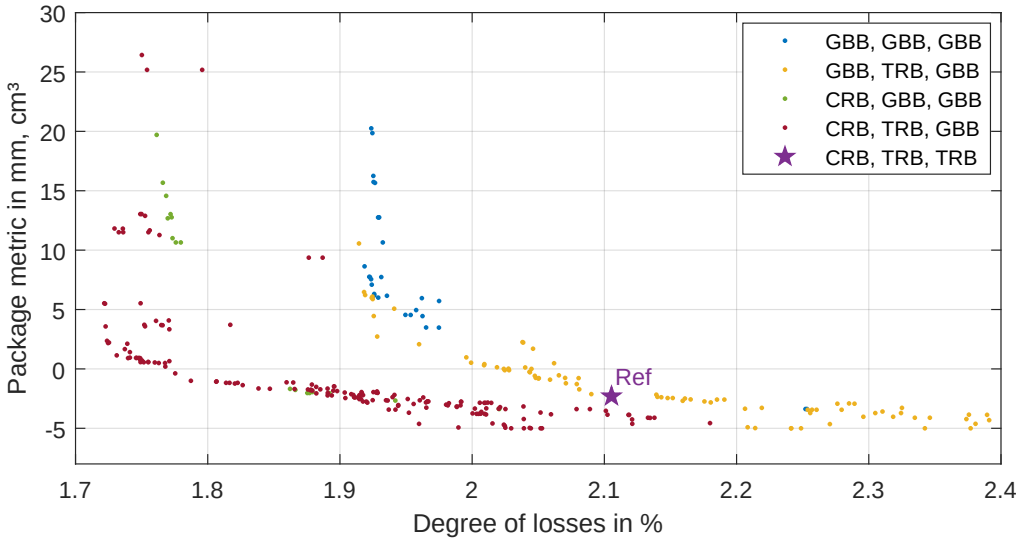

Figure 4.16: Projection of the Pareto front in the dimensions "package metric" and "losses" for case study B (only solutions with a package metric smaller than 30 cm^3 are shown)

5 Conclusion & Outlook

A computer-aided design method for gearboxes in electric vehicles based on a multi-objective optimization approach is presented, which is intended to support the product development process in the early stages. The design process is performed on system level "gearbox" and thus considers all relevant interactions of single subsystems and components to find global optimal gearbox configurations. Furthermore, a detailed package analysis method based on 3D-CAD models of the given installation space, gearbox, electric machine and power electronics is described. The obtained package rating can be directly used as an optimization objective for the gearbox design method, meaning among costs, degree of efficiency and other gearbox properties, the package integration is optimized. To ensure a high accuracy of the results, current industry standards and guidelines are used for the gearbox analysis. The method is demonstrated based on two case studies and the resulting solution sets compared to corresponding reference designs, which represent fully engineered solutions synthesized by means of conventional design strategies. Solutions comparable to the reference designs are present in the solution sets but also various improvement options regarding the optimization objectives are shown.

To further enhance the holistic nature of the approach, a refinement of the described analysis models is of interest. Especially investigations concerning the NVH-behavior of the gearbox system may be covered in greater detail. Furthermore, an extension of the cost model to consider concurrent design problems and already existing designs is of interest to include platform aspects. Finally, comparable design synthesis strategies for the electric machine and power electronics are needed to obtain a design method capable of designing the top-level system "e-drive" in a similar manner. These aspects need to be addressed in future research work.

It can be concluded that the described design method is able to support the decision-making in the early development stages. The multi-objective optimization approach lowers the perceived complexity of the design problem, meaning a reduced development time and risk as well as increased efficiency and effectiveness can be expected. These aspects are vital to pave the way towards clean mobility and handle the challenges originating from the EV-market – today and in the future.

List of Figures

List of Tables

Bibliography

[1] Anteil der Verkehrsträger an den weltweiten CO2-Emissionen aus der Verbrennung fossiler Brennstoffe im Jahr 2014. https://de.statista.com/statistik/daten/studie/317683/umfrage/verkehrsttraeger-anteil-co2-emissionen-fossile-brennstoffe/. [Online; accessed 04 December 2018].

[2] Anzahl verkaufter Elektroautos in Europa im Jahr 2017 nach Modellen. https://de.statista.com/statistik/daten/studie/431419/umfrage/anzahl-verkaufter-elektroautos-in-europa/. [Online; accessed 27 December 2018].

[3] Technische Grundlagen und Produktdaten zur Gestaltung von Wälzlagerungen. https://www.at.schaeffler.com/remotemedien/media/_shared_media/08_media_library/01_publications/schaeffler_2/catalogue_1/downloads_6/hr1_de_de.pdf, 2014. [Online; accessed 28 January 2018].

[4] Electric Vehicles. https://bnef.turtl.co/story/evo2018/, 2018. [Online; accessed 04 December 2018].

[5] L. C. Altherr, T. Ederer, M. E. Pfetsch, et al. Maschinelles Design eines optimalen Getriebes. *Automobiltechnische Zeitschrift*, 120(10):72–77, 2018.

[6] J. S. Arora. Formulating Design Problems as Optimization Problems. *Encyclopedia of Aerospace Engineering*, 2010.

[7] M. Chandrasekaran, S. Padmanabhan, and V. Srinivasa Raman. Single Speed Gearbox Optimization Using Genetic Algorithm. *ARPN Journal of Engineering and Applied Sciences*, 10(13):5506–5511, 2015.

[8] T. H. Chong and J. S. Lee. A Design Method of Gear Trains Using a Genetic Algorithm. *International Journal of the Korean Society of Precision Engineering*, 1(1):62–70, 2000.

[9] K. Deb and S. Jain. Multi-Speed Gearbox Design Using Multi-Objective Evolutionary Algorithms. *Journal of Mechanical Design*, 125(3):609, 2003.

[10] DIN 3960: Begriffe und Bestimmungsgrößen für Stirnräder (Zylinderräder) und Stirnradpaare (Zylinderradpaare) mit Evolventenverzahnung. Standard, Deutsches Institut für Normung, 1987.

[11] M. Eghtessad. *Optimale Antriebsstrangkonfigurationen für Elektrofahrzeuge*. PhD thesis, Technische Universität Braunschweig, 2014.

[12] K. Ehrlenspiel, A. Kiewert, U. Lindemann, et al. *Kostengünstig Entwickeln und Konstruieren*. Springer-Verlag Berlin Heidelberg, 2014.

[13] R. Fischer, F. Küçükay, G. Jürgens, et al. *Das Getriebebuch*. Springer Fachmedien Wiesbaden, 2014.

[14] M. Hofstetter, M. Hirz, and M. Ackerl. System Design Optimization of xEV-Axle Drives with Package Restrictions. In *FISITA 2016 World Automotive Congress*, pages 2846–2855, 2016.

[15] M. Hofstetter, M. Hirz, M. Gintzel, et al. Multi-Objective System Design Synthesis for Electric Powertrain Development. In *IEEE Transportation Electrification Conference and Expo*, pages 286–292, 2018.

[16] M. Hofstetter, D. Lechleitner, M. Hirz, et al. Multi-objective gearbox design optimization for xEV-axle drives under consideration of package restrictions. *Forschung im Ingenieurwesen*, 82(4):361–370, 2018.

[17] L. Horváth and I. Rudas. Driving Engineering Model Generation on Functional and Logical Levels. In *New Trends in Intelligent Software Methodologies, Tools and Techniques - Proceedings of the 16th International Conference, SoMeT 2017*, pages 678–690. IOS Press, 2017.

[18] KISSsoft Inc. KISSsoft 03/2018. `https://www.kisssoft.ch/`.

[19] The MathWorks Inc. Matlab R2017b. `https://de.mathworks.com/products/matlab/`.

[20] ISO 6336: Calculation of load capacity of spur and helical gears. Standard, International Organization for Standardization, 2006.

[21] D. R. Jones, C. D. Perttunen, and B. E. Stuckman. Lipschitzian optimization without the Lipschitz constant. *Journal of Optimization Theory and Applications*, 79(1):157–181, 1993.

[22] M. Köhler, S. Jenne, K. Pötter, et al. *Load Assumption for Fatigue Design of Structures and Components*. Springer-Verlag GmbH Germany, 2017.

[23] U. Kissling. Gearbox Design for tight Space Constraints with simultaneous Cost Estimation. KISSsoft Inc.

[24] B. Künne et al. *Köhler/Rögnitz Maschinenteile 2*. Vieweg+Teubner Verlag, 2008.

[25] S. Koziel, X. Yang, et al. *Computational Optimization*. Springer-Verlag Berlin Heidelberg, 2011.

[26] H. Linke, J. Börner, R. Heß, et al. *Cylindrical Gears*. Carl Hanser Verlag, 2016.

[27] M. Maurer, H. Winner, et al. *Automotive Systems Engineering*. Springer-Verlag Berlin Heidelberg, 2013.

[28] J. Nelder and R. Mead. A Simplex Method for Function Minimization. *The Computer Journal*, 7(4):308–313, 1965.

[29] H. Nguyen-Schäfer. *Computational Design of Rolling Bearings*. Springer International Publishing Switzerland, 2016.

[30] J. Parlow, M. Otto, and K. Stahl. From Specification to Gearing - Application Specific Gear Box Design Using an Explicit Design Model. *Konstruktion*, 68(3):64–69, 2016.

[31] S. Pint, N. Ardey, G. Mendl, et al. The new full electric drivetrain from Audi. In *39. Internationales Wiener Motorensymposium*, 2018.

[32] A. Register. *A Guide to MATLAB Object-Oriented Programming*. CRC Press, 2007.

[33] K. Reif et al. *Konventioneller Antriebsstrang und Hybridantriebe*. Vieweg + Teubner Verlag, 2010.

[34] K. Reif, K. E. Noreikat, K. Borgeest, et al. *Kraftfahrzeug-Hybridantriebe*. Springer Vieweg, 2012.

[35] J. Riegel, W. Mayer, Y. van Havre, et al. FreeCAD 0.18.14335. `https://www.freecadweb.org/`.

[36] N. Riquelme, C. Von Lücken, and B. Barán. Performance metrics in multi-objective optimization. In *XLI Latin American Computing Conference (CLEI)*, pages 1–11. IEEE, 2015.

[37] R. C. Sanghvi, A. S. Vashi, H. P. Patolia, et al. Multi-Objective Optimization of Two-Stage Helical Gear Train Using NSGA-II. *Journal of Optimization*, 2014, 2014.

[38] C. Stan. *Alternative Antriebe für Automobile*. Springer-Verlag Berlin Heidelberg, 2015.

[39] Alessandro Stenico. *Werkstoffmechanische Untersuchungen zur Zahnfußtragfähigkeit einsatzgehärteter Zahnräder*. PhD thesis, Technische Universität München, 2007.

[40] R. Storn and K. Price. Differential Evolution – A Simple and Efficient Heuristic for Global Optimization over Continuous Spaces. *Journal of Global Optimization*, 11(4):341–359, 1997.

[41] J. J. Tomick. *On Convergence of the Nelder-Mead Simplex Algorithm for Unconstrained Stochastic Optimization*. PhD thesis, Pennsylvania State University, 1995.

[42] M. Tutuianu, A. Marotta, H. Steven, et al. Development of a Worldwide Harmonized Light Duty Driving Test Cycle (WLTC). Technical report, UNECE, 2013.

[43] J. Weber. *Automotive Development Processes*. Springer-Verlag Berlin Heidelberg, 2009.